FINAL REPORT #00042134-04

GRANT: DTRT13-G-UTC45
Project Period: 09/31/2014 – 05/31/17

Performance of FRCM Strengthened Beams Subject to Fatigue

Participating Consortium Member:
University of Miami

Authors:

Houman A. Hadad
Ph.D. Candidate
Dept. of Civil, Arch. & Environ. Engineering
University of Miami

Vanessa Pino, Ph.D, P.E.
Dept. of Civil, Arch. & Environ. Engineering
University of Miami

Antonio Nanni, Ph.D., P.E.
Professor and Chair
Dept. of Civil, Arch. & Environ. Engineering
University of Miami

RE-CAST:
Research on Concrete Applications for Sustainable Transportation
Tier 1 University Transportation Center

DISCLAIMER

The contents of this report reflect the views of the authors, who are responsible for the facts and the accuracy of the information presented herein. This document is disseminated under the sponsorship of the U.S. Department of Transportation's University Transportation Centers Program, in the interest of information exchange. The U.S. Government assumes no liability for the contents or use thereof.

TECHNICAL REPORT DOCUMENTATION PAGE

1. Report No. RECAST UTC #00042134-04	**2. Government Accession No.**	**3. Recipient's Catalog No.**
4. Title and Subtitle Performance of FRCM Strengthened Beams Subject to Fatigue		**5. Report Date** May 31, 2017
		6. Performing Organization Code:
7. Author(s) H. A. Hadad, V. Pino, and A. Nanni		**8. Performing Organization Report No.** Project #00042134-04
9. Performing Organization Name and Address RE-CAST - University of Miami 1251 Memorial Drive, Room 325 Coral Gables, FL 33146-0630		**10. Work Unit No.**
		11. Contract or Grant No. USDOT: DTRT13-G-UTC45
12. Sponsoring Agency Name and Address Office of the Assistant Secretary for Research and Technology U.S. Department of Transportation 1200 New Jersey Avenue, SE Washington, DC 20590		**13. Type of Report and Period Covered:** Final Report Period: 09/30/2014 – 12/31/16
		14. Sponsoring Agency Code:

15. Supplementary Notes
The investigation was conducted in cooperation with the U. S. Department of Transportation.

16. Abstract
Fabric Reinforced Cementitious Matrix (FRCM) systems have been developed to strengthen or rehabilitate existing concrete and masonry structures subject to damage, steel reinforcement corrosion or requiring resistance capacity improvements due to increased service loads or upgraded code requirements. Bridge decks, girders and pile caps, and parking structures are subject to cyclic loads caused by moving vehicles and, therefore, experience the fatigue phenomenon. Accordingly, this project is aimed at investigating the parameters that most influence the fatigue performance of Carbon- and PBO-FRCM strengthened elements and, in particular, flexure-deficient reinforced concrete (RC) beams. The proposed work includes material characterization of both PBO-FRCM and Carbon-FRCM systems and experimental testing of RC beams strengthened with FRCM subject to static and fatigue loading. As an outcome, the stress ratio vs. number of cycles (S-N curve) that specimens endured before failure was established for each strengthening system.

17. Key Words Fatigue; FRCM; reinforced concrete; repair	**18. Distribution Statement** No restrictions. This document is available to the public.	
19. Security Classification (of this report) Unclassified	**20. Security Classification (of this page)** Unclassified	**21. No of Pages** 53

Form DOT F 1700.7 (8-72) Reproduction of form and completed page is authorized.

PERFORMANCE OF FRCM STRENGTHENED BEAMS SUBJECT TO FATIGUE

PREPARED FOR THE
UNIVERSITY TRANSPORTATION CENTER

Written By:
Houman A. Hadad, Ph.D Candidate
Vanessa Pino, Ph.D, P.E.
Antonio Nanni, P.E., Professor and Chair
Department of Civil, Arch. and Environ. Engineering

UNIVERSITY OF MIAMI
RE-CAST

Submitted
May 31, 2017

PERFORMANCE OF FRCM STRENGTHENED BEAMS SUBJECT TO FATIGUE

EXECUTIVE SUMMARY

Fabric reinforced cementitious matrix (FRCM) systems have emerged as novel strengthening technologies. FRCM is a composite material consisting of a sequence of one or more layers of cement-based matrix reinforced with dry-fiber fabric(s).

The main purpose of the study was an extensive material characterization of two pre-selected FRCM systems, namely: PBO-FRCM and Carbon-FRCM, and using these experimental properties in order to determine the performance of these composites under cyclic loading when applied to reinforced concrete (RC) beams. In the flexure tests investigation, the objective was to ascertain the threshold of applied stress that prevents premature failure due to cyclic loading known as the fatigue endurance limit.

Material characterization and design of strengthening systems are performed in compliance with established Acceptance Criteria AC434-13 (issued by International Code Council Evaluation Service (ICC-ES)) and American Concrete Institute (ACI) design guide ACI 549.4R-13. Results from the characterization yield material properties that are considered in determining experimental, theoretical, and design ultimate capacities of strengthened RC members. Material characterization of all the components including the steel reinforcement and the concrete itself were obtained experimentally and used in place of nominal values provided by manufacturers. Parameters affecting the fatigue performance (e.g., FRCM reinforcement ratio) were investigated and the failure modes of the strengthened RC beams were studied and commented on. Customary to fatigue-related research, the stress ratio vs. number of cycles (S-N curve) that beams endured before failure was established for each strengthening system. All the characterization and RC beam experiments were conducted at University of Miami Structures and Materials Laboratory.

ACKNOWLEDGMENTS

The project was made possible with the financial support received from the University Transportation Center and the Qatar Foundation. The authors gratefully acknowledge the extensive help received during the experimental work by students, staff and faculty at the University of Miami. The opinions in this report are those of the authors and not necessarily those of the sponsors or collaborators.

TABLE OF CONTENTS

LIST OF FIGURES

LIST OF TABLES

1 INTRODUCTION

1.1 Background

1.1.1 Fabric Reinforced Cementitious Matrix (FRCM) Composites

Fabric reinforced cementitious mortar (FRCM) recently emerged as an additional strengthening technology due to its inherent heat resistance and compatibility with the substrate (i.e., can be applied on a wet surface and allow vapor permeability). FRCM systems consist of one or more layers of dry fabrics made of Carbon, Glass, Aramid, or Polyparaphenylene benzobisoxazole (PBO) fibers that are sandwiched between layers of cementitious mortars (Figure 1.1-1). Dry fabrics imply that the fibers are not fully impregnated by the matrix, contrary to FRP systems. Fabrics are produced with various fiber strand sizes and spacings and the lightweight, high tensile strength, and ease of application makes the system appealing. The cement-based matrix having high compressive strength but low tensile strength has the function of protecting and transferring the load to the fibers. Therefore, the fibers are the primary tensile load carrying mechanism. Even though some interesting field applications have been reported that justify FRCM potential as a strengthening technology, experimental and theoretical research is still needed to fully characterize FRCM and quantify its mechanical effectiveness.

The current criteria used to evaluate, characterize, and approve FRCM composite systems for strengthening existing masonry and concrete structures was developed by the International Code Council Evaluation Service (ICC-ES). This document is titled: AC434-2013–"Acceptance Criteria for Masonry and Concrete Strengthening Using Fabric-Reinforced Cementitious Matrix (FRCM) Composite Systems", and it states the guidelines for standards and test procedures required to evaluate products for code compliance. Similarly, the current design and construction guidelines for FRCM systems was developed by the American Concrete Institute (ACI) and is titled ACI 549.4R-13 "Guide to Design and Construction of Externally Bonded Fabric Reinforced Cementitious Matrix (FRCM) Systems for Repair and Strengthening Concrete and Masonry Structures" (ACI 549.4R 2013). This document also contains all necessary tools for an effective design and construction of FRCM systems: material properties, system qualification, installation guidelines, design considerations for both reinforced concrete and masonry, reinforcement details, and design examples.

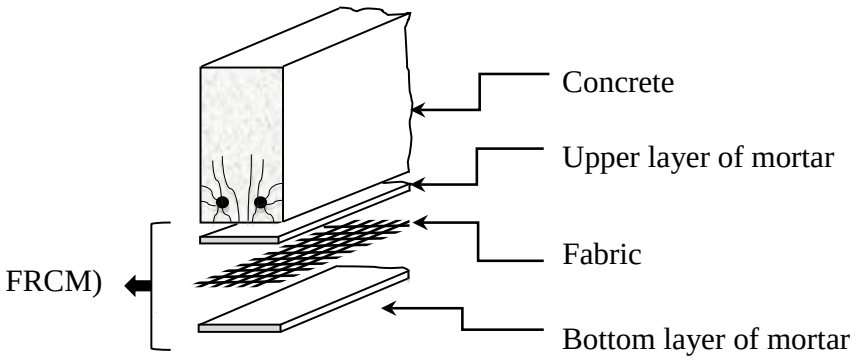

Figure 1.1-1– Schematic representation of FRCM for strengthening concrete structures

1.2 Objectives

The overall aim of this research is to contribute new evidence to the functionality, integrity, and compatibility of FRCM systems with the strengthened structure. In particular, the objective is to investigate the basic constitutive behavior and durability of FRCM systems as well as the parameters that most influence the fatigue flexural performance of strengthened RC beams. Based on these parameters, t a fatigue endurance limit can be determined to be proposed to the institutional guidelines for the design of externally bonded FRCM strengthening systems.

2 FRCM MATERIAL CHARACTERIZATION

2.1 Materials

2.1.1 Fabric Reinforced Cementitious Matrix (FRCM)

Two FRCM materials are proposed for this project. The first one is a Carbon FRCM system with two fabric architectures, namely: C600 (unidirectional) and C200 (bidirectional) as shown in Figure 2.1-1. The unidirectional carbon fabric has a tow (yarn) cross-sectional area equivalent to 2.5 mm^2 (0.00387 in^2) with a yarn spacing given in Figure 2.1-1-a, while the bidirectional carbon fabric has a tow (yarn) cross-sectional area equivalent to 0.88 mm^2 (0.00136 in^2) with a yarn spacing as given in Figure 2.1-1-b. Both systems are used with the cementitious mortar (CM) provided by the manufacturer. Material Characterization of the Carbon FRCM system is explained herein.

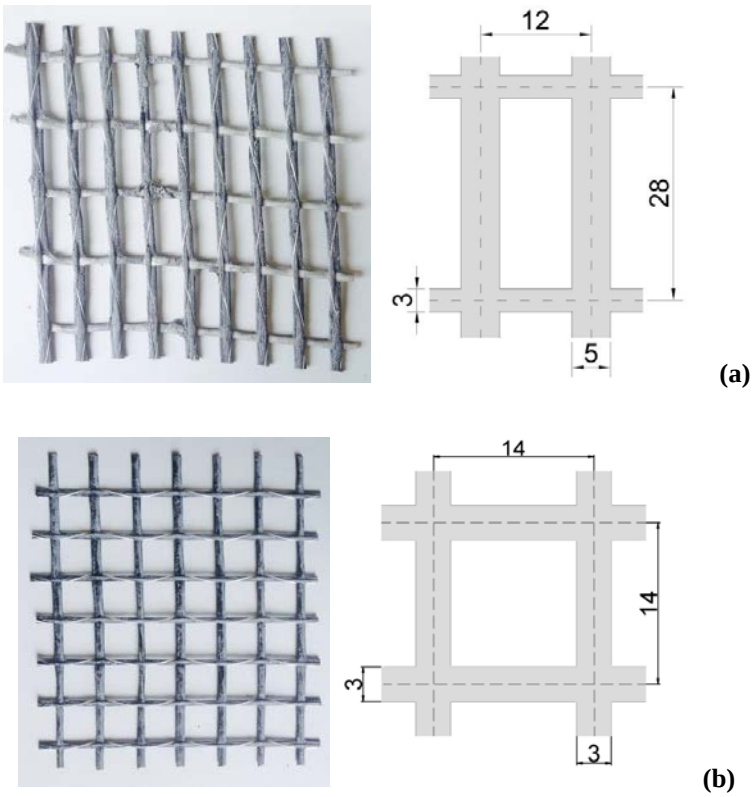

Figure 2.1-1– Carbon FRCM systems: (a) unidirectional fabric (C600); (b) bidirectional fabric (C200)

The other one is a polyparaphenylene benzobisoxazole (PBO) fabric (X Mesh Gold (GOLD)) embedded in a matrix identified as X Mortar 750 (M750). GOLD is an unbalanced network made of 10 and 20 mm (0.4 and 0.8 in.) spaced fiber rovings. The free space between rovings is roughly 5 and 15 mm (0.2 and 0.6 in.), respectively, and the nominal thickness in the two fibers directions is 0.046 mm (0.0018 in.) in the primary direction and 0.01 mm (0.0004 in.) in the secondary direction, refer to Figure 2.1-2. M750 is a stabilized inorganic cementitious matrix used for concrete flexural and shearing stress reinforcement. Material characterization of PBO FRCM was previously reported in ***RE-CAST REPORT #00042134-04: FRCM and FRP Composites for the Repair of Damaged PC Girders*** *by Pino and Nanni*.

a) b) c)

Figure 2.1-2 – FRCM material constituents: a) GOLD fabric roll; b) GOLD fabric; c) M750 mortar

2.2 Carbon FRCM Preparation and Installation

2.2.1 Mixing Method

The inorganic matrix product is prepared by mechanical mixing, since hand mixing is not suggested by the manufacturer. The preparation initiates by adding the dry powder cementitious matrix to 90% of the water needed for the mix. Mixing continues for at least 3 minutes until creating a homogeneous matrix paste. If necessary, the remaining 10% water is added and mixed for an additional 2 minutes. Upon completion, the mortar rests for 2 minutes before being applied to the substrate surface.

2.2.2 Mixing Ratio

The cementitious mortar mix to water ratio used per manufactures instructions was in the range of 2.7 to 3 kg (6 to 6.5 lb.) of water per 22.7 kg (50 pound) bag of dry mix.

2.2.3 Specimen Preparation

Step 1:

Cut fabrics with the desired panel dimensions: nominally 580x450 mm (23x18 in.) as seen in Figure 2.2-1. The fabric is flattened due to its initial curvature, caused by the method of shipping in a roll. Typically, this is not required when installing the FRCM system in actual repair applications that involve larger areas of installation.

Step 2:

Mortar is mixed (dry power to water) per manufacturer's instructions as reported in section 2.2.1, and seen in Figure 2.2-1.

(a) (b)

Figure 2.2-1– (a) Cut and flattened fabric of FRCM system; and (b) mixing of the FRCM mortar

Step 3:

Apply the first layer of mortar with a trowel on a bond-free flat surface with a thickness of 3.0 to 4.0 mm (0.12 to 0.16 in.), while removing any excess on the sides, as seen at the start of the sequence of photos given in Figure 2.2-2.

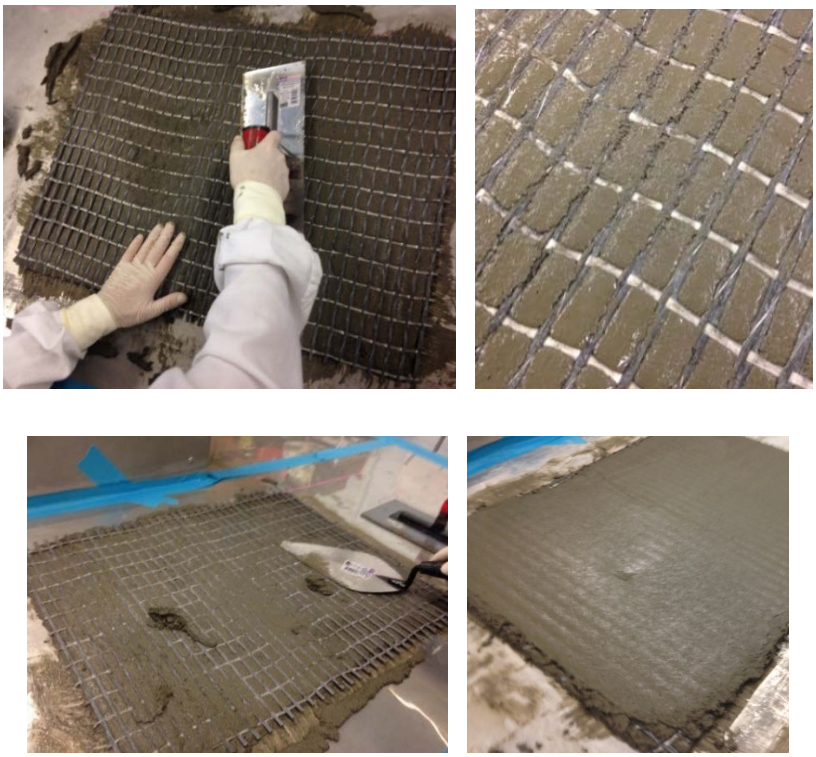

Figure 2.2-2– FRCM panel fabrication: steps 3 to 5

Step 4:

Lay the pre-cut flat fabric with the desired orientation on the first layer of the mortar, while pressing lightly with the trowel to embed the fabric in the upper part of the first mortar layer, as seen in the sequence photos of Figure 2.2-2.

Step 5:

Add a second layer of the mortar with the trowel to cover the fabric with a thickness of 3.0 to 4.0 mm (0.12 to 0.16 in.).

2.2.4 FRCM Installation Procedure (Substrate)

For specimens that included a substrate (e.g., bond testing), the FRCM systems were installed on a concrete substrate. The surface preparation before the installation of the FRCM systems included sandblasting, pressure cleaning and wetting to attain a saturated surface-dry (SSD) condition. The installation of the FRCM on a substrate followed the same steps as previously described.

2.3 Test Matrix

A comprehensive summary of the test matrix for Carbon FRCM characterization is given in Table 2.3-1.

Table 2.3-1 – FRCM material characterization test matrix

Test	Reinforcement		Conditioning		Replicates	Specification
	Fabric	Plies	Environment	Duration		
Compression of Matrix Mortar	None	n/a	Lime water	7 days	5	ASTM C109
				28 days	5	ASTM C109
FRCM Direct Tension	Continuous	One	Ambient	n/a	5	AC434 Annex A
	Continuous	Two	Ambient	n/a	5	AC434 Annex A
	Lap	One	Ambient	n/a	5	AC434 Annex A
FRCM Interlaminar Shear	Continuous	One	Ambient	n/a	5	ASTM D2344
		Two	Ambient	n/a	5	ASTM D2344
FRCM bond over Repair Mortar	Continuous	One	Ambient	n/a	5	ASTM C1583
FRCM Bond	Continuous	One	Ambient	n/a	5	ASTM C1583
FRCM Bond	Continuous	One	Saltwater	1000 hrs. 3000 hrs.**	5 5	ASTM C1583 ASTM D1141
FRCM Bond	Continuous	One	Water vapor	1000 hrs. 3000 hrs.**	5 5	ASTM C1583 ASTM D2247
FRCM Bond	Continuous	One	Alkaline	1000 hrs. 3000 hrs.**	5 5	ASTM C1583 ASTM C581

** Post Testing

2.4 Test Data and Results

2.4.1 Mortar Compressive Strength

The purpose of this test is to evaluate the compressive strength of mortar used for FRCM strengthening application as per AC434-Section 4.3 and reference standard ASTM C109/C109M. Ten (10) -51 mm (2 in) cube samples were cast in cube molds as per ASTM C109. Cube specimens were prepared by hand tamping the mortar in two layers, after mechanically mixing the mortar. Immediately upon completion of molding, the mold was placed in a moist room to cure for 24 hours with their upper surface of the specimens exposed to the moist air but protected from dripping water. Specimens were removed from the molds after the first day of curing (Figure 2.4-1) and exposed to a limewater conditioning environment for 7 and 28 days, five samples for each conditioning time (Figure 2.4-2).

Figure 2.4-1–Cube de-molding for compressive strength of mortar tests

Figure 2.4-2–Cubes in limewater conditioning

Uniaxial compression load was applied to each cube using a screw type universal test frame as seen in Figure 2.4-3. Load was applied to the cube faces that were in contact with the mold surfaces. The test was performed under displacement control at a rate of 0.635 mm/minute (0.025 in./min). All cubes failed by crushing as shown in Figure 2.4-4.

Required minimum compression breaking strengths are 17 MPa (2,500 psi) at 7 days of age and 24 MPa (3,500 psi) at 28 days of age (AC434 Section 4.3). The cube compressive strength (f'_c) was determined by dividing the peak load (P_{max}) by the average area (A) of the faces of the cube in contact with the loading platens. A summary of all results is given in Table 2.4-1.

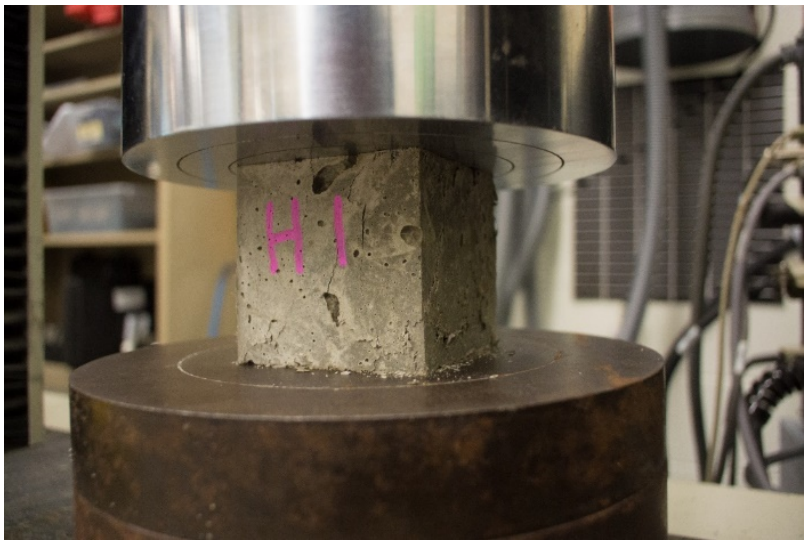

Figure 2.4-3 –Cube compression test

Table 2.4-1 – Summary of mortar compressive strength results

SPECIMEN ID	Ave. Area	Peak Load		Compressive Strength	
	in^2	kN	lb.	MPa	psi
STi-CM-CSM-CC-07-01	4.00	97.37	21880	37.74	5470
STi-CM-CSM-CC-07-02	4.00	99.15	22280	38.43	5570
STi-CM-CSM-CC-07-03	4.00	103.60	23280	40.15	5820
STi-CM-CSM-CC-07-04	4.00	109.92	24700	42.60	6175
STi-CM-CSM-CC-07-05	4.00	106.44	23920	41.26	5980
Average		103.29	23212	40.04	5803
S_{n-1}		5.15	1158	2.00	289
CV((%)		4.99	4.99	4.99	4.99
STi-CM-CSM-CC-28-01	4.00	117.12	26320	45.40	6580
STi-CM-CSM-CC-28-02	4.00	122.51	27530	47.48	6883
STi-CM-CSM-CC-28-03	4.00	118.95	26730	46.10	6683
STi-CM-CSM-CC-28-04	4.00	117.04	26300	45.36	6575
STi-CM-CSM-CC-28-05	4.00	120.77	27140	46.81	6785
Average		119.28	26804	46.23	6701
S_{n-1}		2.37	532	0.92	133
CV((%)		1.99	1.99	1.99	1.99

Figure 2.4-4–Representative failure mode of compression test cubes

2.4.2 FRCM Direct Tension

The purpose of this test is to determine tensile strength, elongation, and modulus of elasticity of the FRCM system using coupons tested under ambient conditions. Tensile coupons were tested as per AC434 Section 4.2.3 according to Annex A: Tensile Testing of FRCM Composite Specimens (AC434 2013).

Panels were made using a flat mold with non-adhesive surface surrounded by rectangular aluminum rods to control the overall thickness of the panel. FRCM installation followed the description provided in Section 2.2 of this report. Panels having Length x Width dimentions of 410 x 560 mm (16 x 22 in.) were left to cure for 28 days before coupons were extracted with a circular diamond blade saw from the panels. Coupons were cut with a nominal size of 410 x 50 mm (16 x 2 in) length x width, respectively. Fiber alignment was set in the 0° direction along the length of the coupon for both fabric types. C600 specimens had a single layer of fabric, while C200 specimens had two layers of fabric for all tests.

The saw was equipped with a rigging fixture to ensure coupons were secured and cut to the specified dimensions. The specimens were prepared as described in Section 2.2. Steel metal tabs of 150 mm (6 in.) length were adhesively bonded to the FRCM ends with epoxy, which was cured for at least 24 hrs. prior to testing. During adhesion of the tabs, specimens were set on a fixture frame to ensure tab/specimen alignment and location of the clevis openings as seen in Figure 2.4-5.

Figure 2.4-5-Tensile specimen preparation set up

Lap tensile strength coupon specimens were made following the same methodology, with the difference being a nominal fabric overlap length of 120 mm (4.72 in). Steel metal tabs with clevis openings were bonded to each end of the specimen with Loctite PL Premium Polyurethane Construction Adhesive. The tab lengths were 150 mm (6 in) for one and two-ply continuous tensile coupons and 100 mm (4 in) for the single ply lap tensile coupons. The glue cured for at least 24 hours prior to testing. During gluing, coupons were set on a frame to ensure tab alignment and location of the clevis openings as seen in Figure 2.4-6.

All specimens were conditioned prior testing under laboratory ambient conditions at room temperature 23 ± 3°C (73 ± 6°F) and 60 ±5% relative humidity, for at least 28 days.

Uniaxial tension load was applied to the tensile coupons. Testing was performed using a screw driven Instron Universal Test Frame with a maximum capacity of 130 kN (30 kip). Axial deformation was measured using a clip on extensometer with a 100 mm (4 in) gauge length, placed at mid-length of the specimen. The gripping mechanism is a clevis-type connection on one end and a double clevis connection on the other end (Figure 2.4-7). This ensures boundary conditions that maximize the degrees of freedom, minimize bending, and simulate actual conditions in the field. All data was gathered using Instron's Bluehill software and data acquisition system. Figure 2.4-8 shows the multiple crack pattern in a cracked specimen.

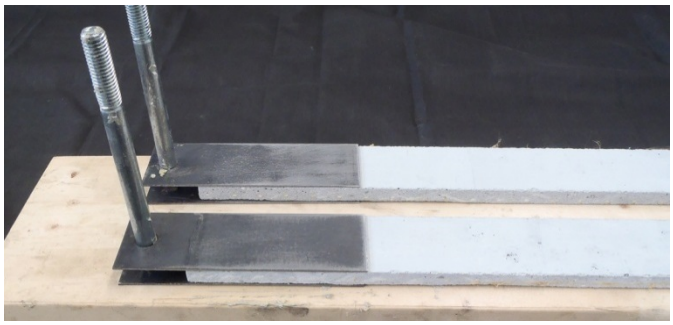

Figure 2.4-6 – Tab installation

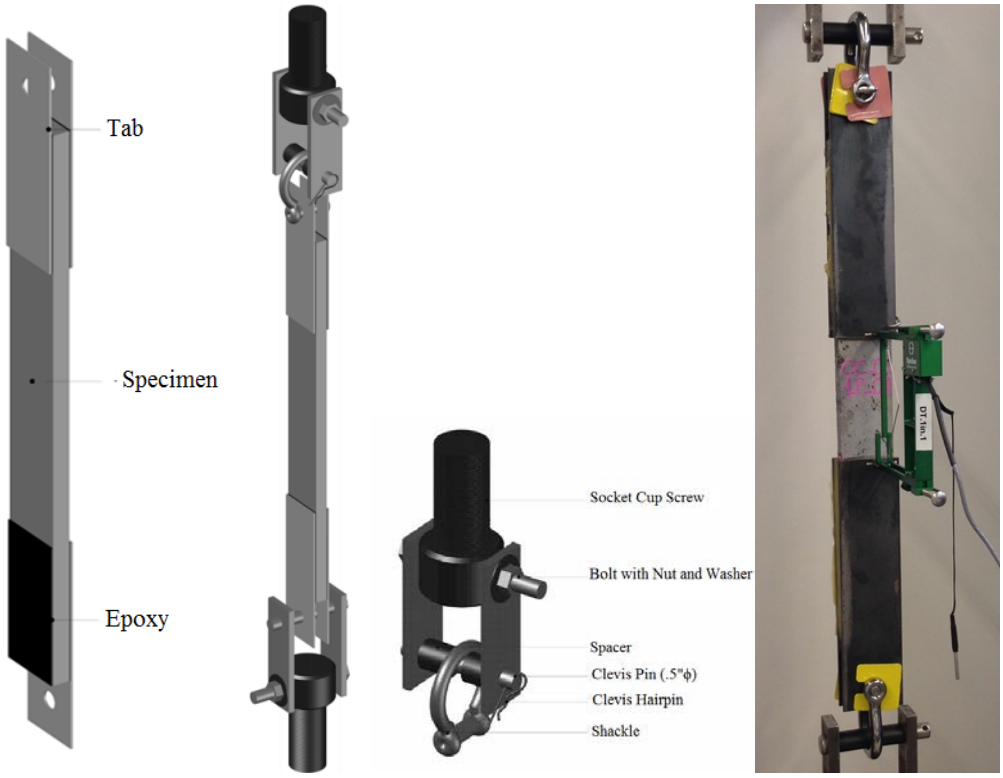

Figure 2.4-7–Specimen test setup with clevis grips and extensometer

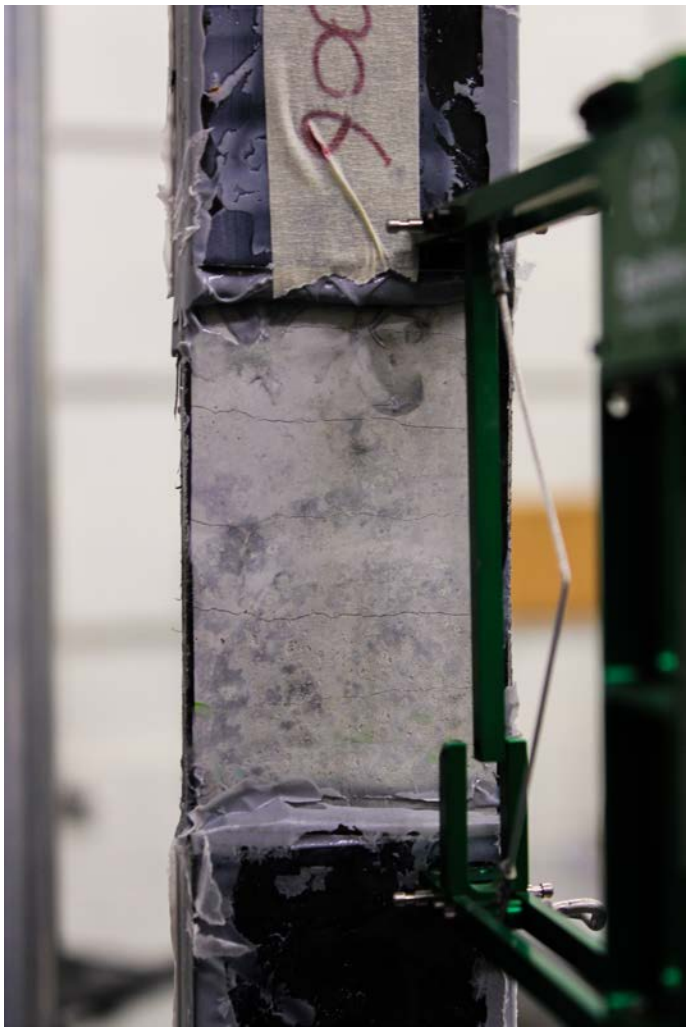

Figure 2.4-8 – Crack propagation in tensile coupons

The test was performed under displacement control at a rate of 0.25 mm/minute (0.01 in./min). An initial pre-tension load of 0.10 kN (22 lb), less than 5% of ultimate capacity, was applied to engage the specimen and clevis grip setup. The stress-strain behavior of FRCM control coupon specimens is bi-linear as expected. The initial branch of the curve corresponds to the un-cracked specimen, followed by a second branch with a reduced slope, corresponding to the cracked specimen. For the continuous and lap splice specimens, the primary failure mode was slippage of the fibers after multiple cracking throughout the length of the specimen, perpendicular to the direction of the load. A secondary debonding failure mode located at the tab ends was observed in some cases.

Cracking begins where a crack spans the entire width of the specimen, then the crack begins to propagate through the thickness. In some instances, instead of propagating through the entire thickness, the crack propagates through the first layer of fabric and then runs parallel to the length

of the specimen. This phenomenon is more pronounced for specimens with high fiber volume. The modulus of the cracked and un-cracked specimen is determined from the stress-strain curves (see Figure 2.4-9) as follows:

Modulus of the cracked specimen: On the segment of the response curve corresponding to cracked behavior after the transition as defined in AC434 A7.2, two points are selected on the experimental curve at a stress level equal to $0.90f_{fu}$ and $0.60f_{fu}$. The slope of the line that connects these two points represents the tensile modulus of elasticity at that region:

$$E_f = \Delta f / \Delta \varepsilon = (0.90\ f_{fu} - 0.60\ f_{fu}) / (\varepsilon f@0.90\ f_{fu} - \varepsilon f@0.60\ f_{fu})$$

Modulus of the un-cracked specimen: It is calculated using the slope between two points. The first point is the origin. The second point is the intersection of the linear trend of the first portion of the experimental curve and the linear trend of the second portion of the experimental curve.

Table 2.4-2 contains the average tabulated stress, strain and elastic modulus results with average, standard deviation (Std. Dev.) and coefficient of variance (C.O.V) values for the single ply and two-ply direct tension tests on C600 and C200 FRCM coupons, where the following nomenclature (as specified in AC434) was used:

- Ef^* Modulus of elasticity of the un-cracked specimen;
- E_f Modulus of elasticity of the cracked specimen;
- f_{ft} Tensile stress corresponding to the transition point;
- ε_{ft} Tensile strain corresponding to the transition point;
- f_{fu} Ultimate tensile strength; and
- ε_{fu} Ultimate tensile strain.

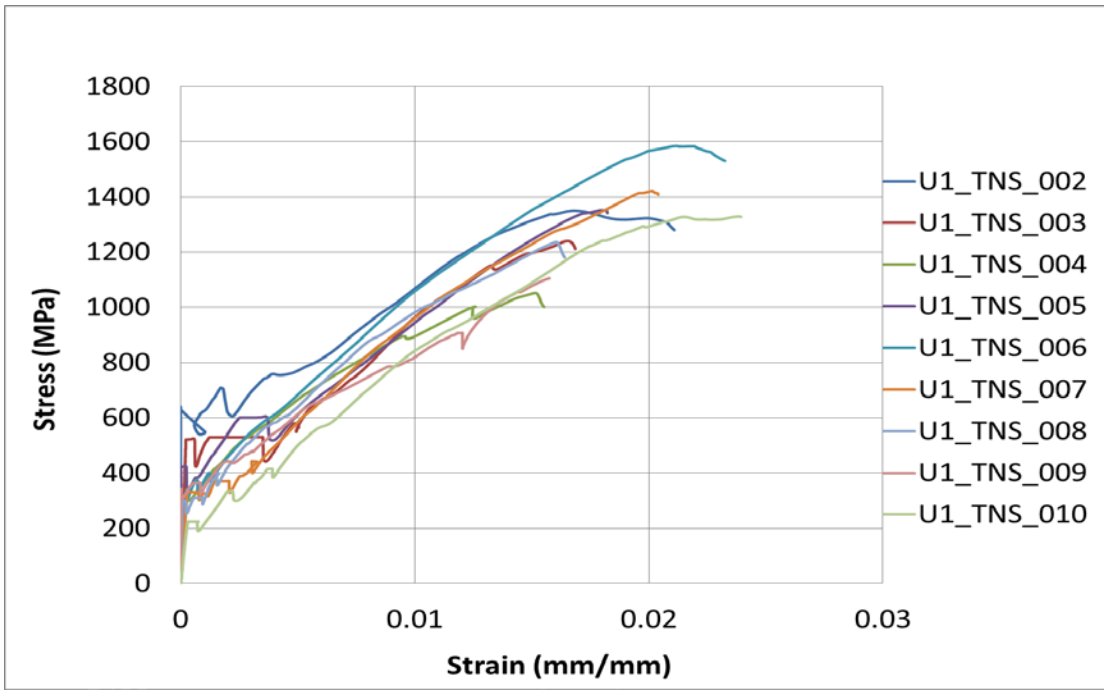

Figure 2.4-9– Representative results for direct tension specimens

Similarly, Table 2.4-3 represents the average tabulated stress, strain and elastic modulus results with average, standard deviation (Std. Dev.) and coefficient of variance (C.O.V) values for the single ply and two-ply lap specimen tests on C600 and C200 FRCM coupons.

Table 2.4-2– Tabulated direct tensile strength tests per AC434 Annex A

SPECIMEN ID	Yarn	Peak Load		Ultimate Strength		Modulus of Elasticity Cracked		Modulus of Elasticity Uncracked		Ultimate Strain	Transition point Strength		Transition point Strain
	#	kN	lbf	MPa	ksi	GPa	Msi	GPa	Msi	%	MPa	ksi	%
STi_C600_TNS _00_001	3	11.88	2670	1584	229.7	59.10	8.58	1178.1	170.94	1.92	470.39	68.22	0.040
STi_C600_TNS _00_002	3	10.66	2396	1421	206.1	54.90	7.97	1217.0	176.59	1.87	413.39	59.96	0.034
STi_C600_TNS _00_003	3	7.98	1793	1064	154.3	82.70	12.00	1427.0	207.06	0.90	380.00	55.1	0.030
STi_C600_TNS _00_004	3	10.80	2427	1440	208.9	72.20	10.48	1520.0	220.55	1.60	338.00	49.0	0.020
STi_C600_TNS _00_005	3	10.96	2463	1461	211.9	58.60	8.50	1420.0	206.04	1.90	362.00	52.5	0.020
Average		10.46	2350	1394	202.2	65.50	9.50	1352.4	196.24	1.64	392.76	56.96	0.03
S_{n-1}		1.46	329	195	28.3	11.64	1.69	147.4	21.39	0.43	51.38	7.45	0.01
CV((%)		14.0	14.0	14.0	14.0	17.8	17.8	10.9	10.9	26.4	13.1	13.1	30.5
STi_C200_TNS _00_001	5	5.28	1187	1200	174	78	11.25	6185	897	1.00	445.00	64.54	0.010
STi_C200_TNS _00_002	5	5.13	1153	1166	169	52	7.51	5551	805	1.45	420.00	60.92	0.010
STi_C200_TNS _00_003	5	4.57	1027	1039	151	87	12.62	7000	1016	1.05	389.00	56.42	0.010
STi_C200_TNS _00_004	5	5.20	1169	1182	171	55	7.98	5828	846	1.20	517.00	74.98	0.010
STi_C200_TNS _00_005	5	5.10	1146	1159	168	55	7.98	5002	726	1.46	548.00	79.48	0.010

SPECIMEN ID	Yarn	Peak Load		Ultimate Strength		Modulus of Elasticity Cracked		Modulus of Elasticity Uncracked		Ultimate Strain	Transition point Strength		Transition point Strain
	#	kN	lbf	MPa	ksi	GPa	Msi	GPa	Msi	%	MPa	ksi	%
Average		5.06	1136	1149	167	65	9.47	5913	858	1.23	463.80	67.27	0.010
S_{n-1}		0.28	63	64	9	16	2.31	746	108	0.22	66.68	9.67	0.000
CV((%)		5.5	5.5	5.5	5.5	24.4	24.4	12.6	12.6	17.6	14.4	14.4	0.0
STi_C200_TNS _90_001	4	5.87	1319	1668	242	109.75	15.92	2421	351	1.09	n/a	n/a	n/a
STi_C200_TNS _90_002	4	4.82	1083	1369	199	73.76	10.70	2431	353	1.10	n/a	n/a	n/a
STi_C200_TNS _90_003	4	5.06	1137	1438	208	99.15	14.39	2026	294	1.19	n/a	n/a	n/a
STi_C200_TNS _90_004	4	5.23	1175	1486	215	93.31	13.54	2431	353	1.10	n/a	n/a	n/a
STi_C200_TNS _90_005	4	5.53	1243	1571	228	71.75	10.41	2253	327	1.50	n/a	n/a	n/a
Average		5.30	1191	1506	218	89.54	12.99	2312	336	1.20			
S_{n-1}		0.41	92	116	17	16.44	2.38	177	26	0.17			
CV((%)		7.7	7.7	7.7	7.7	18.4	18.4	7.7	7.7	14.6			

Table 2.4-3– Tabulated results for lap specimens per AC434 Annex A

SPECIMEN ID	No.of Yarns	Peak Load		Ultimate Strength		Ultimate Strength Retention *
	#	kN	lbf	MPa	ksi	%
STi_C600_LTS _08_001	3	9.90	2225	1320.0	191.4	95
STi_C600_LTS _08_002	3	10.64	2391	1418.7	205.8	102
STi_C600_LTS _08_003	3	10.90	2449	1453.3	210.8	104
STi_C600_LTS _08_004	3	11.20	2517	1493.3	216.6	107
STi_C600_LTS _08_005	3	11.48	2580	1530.7	222.0	110
Average		10.82	2432	1443.2	209.3	104
S_{n-1}		0.61	136	80.7	11.7	6
CV((%)		5.6	5.6	5.6	5.6	5.6
STi_C200_LTS _06_001	4	7.30	1640	1381.00	200.30	120
STi_C200_LTS _06_002	4	4.44	998	1261.00	182.89	110
STi_C200_LTS _06_003	4	5.23	1175	1080.00	156.64	94
STi_C200_LTS _06_004	4	6.84	1537	1555.00	225.53	135
STi_C200_LTS _06_005	4	6.16	1384	1400.00	203.05	122
Average		5.99	1347	1335.40	193.68	116
S_{n-1}		1.17	262	176.95	25.66	15
CV((%)		19	19	13	13	13

**Condition of acceptance is equivalent to more than 100% retention compared to direct tensile strength*

2.4.3 Interlaminar Shear Strength

The purpose of this test is to evaluate the interlaminar shear strength of the FRCM composite system under control ambient conditions. Tests are performed as per AC434 Section 4.2.4 and reference standard ASTM D2344/D2344M-00 (2006) “Standard Test Method for Short-Beam Strength of Polymer Matrix Composite Materials and Their Laminates.” The nominal rectangular

prism specimen dimensions are 70 x 25 x 12.5 mm (2.75 x 1 x 0.5 in.) with a single ply of each FRCM system fabric (see Figure 2.4-10).

Figure 2.4-10 –Interlaminar shear specimen

The specimen was loaded in three-point bending. Testing was performed using a screw driven Instron Universal Test Frame with a maximum capacity of 130 kN (30 kip). The load was measured with the internal load cell of the frame in compliance with ASTM E4-10 “Standard Practice for Force Verification of Testing Machines”. The test set-up is shown in Figure 2.4-11. Load and crosshead displacement were recorded throughout the test using the Instron’s Bluehill software and data acquisition system. Load was applied in displacement control at a constant frame head displacement of 1.0 mm/min (0.05 in./min) as per ASTM D2344 requirements.

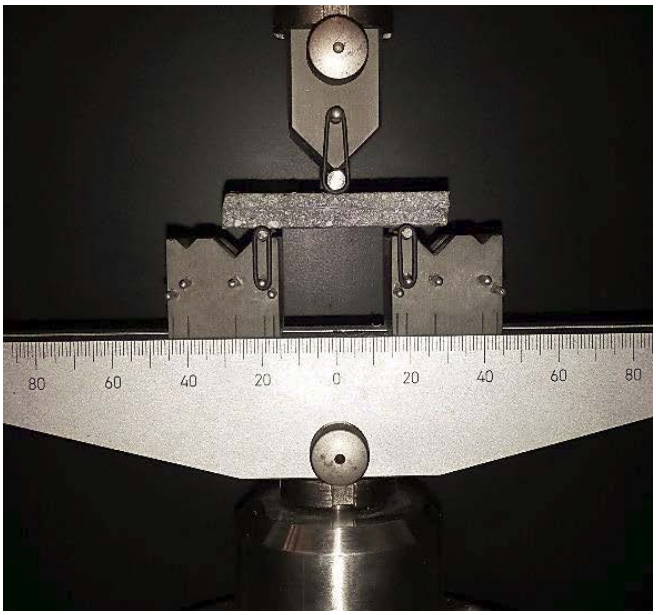

Figure 2.4-11– Interlaminar shear test set-up

The average short beam strength for single ply interlaminar shear is 1.25 MPa (182 psi) and for two-ply interlaminar shear is 2.24 MPa (325 psi) and 2.22 MPa (322 psi) for C600 and C200 FRCM, respectively. The primary failure mode of the FRCM short beam specimens was by matrix cracking originated in the tension side of the coupon, and less often by a combination of cracking and interlaminar shear.

The short beam strength is calculated as follows:

$$F^{sbs} = 0.75\frac{P_m}{bh} \qquad F^{sbs} = 0.75 * \frac{P_m}{b*h}$$

Where:

F^{sbs} is the short beam strength, MPa (psi);
P_m is the maximum load obtained during the test, N (lb).;
b is the measured specimen width, mm (in);
h is the measured specimen thickness, mm (in).

Table 2.4-4 contains tabulated specimen dimensions, maximum load, and short beam strength results with average, standard deviation (Std. Dev.) and coefficient of variance (C.O.V) values.

Table 2.4-4– Interlaminar shear test summary for ambient single ply specimens

Specimen ID	*b*		*h*		P_m		F^{sbs}		Failure Mode
	mm	*in*	mm	*in*	*N*	*lbf*	*MPa*	*ksi*	
STi_C600_ISS _00_01	25	1.02	12.5	0.510	904	203	2.17	315	TF
STi_C600_ISS _00_02	25	1.02	12.5	0.510	911	205	2.19	317	TF
STi_C600_ISS _00_03	25	1.02	12.2	0.498	835	188	2.05	298	TF
STi_C600_ISS _00_04	25	1.02	12.5	0.510	905	203	2.17	315	TF
STi_C600_ISS _00_05	25	1.02	12.4	0.506	1089	245	2.63	382	TF
Average					929	209	2.24	325	
S_{n-1}					94.6	21.3	0.2	32.6	
CV((%)					10.2	10.2	10.0	10.0	
STi_C200_ISS _00_01	24	0.98	11.8	0.482	804	181	2.13	309	TF
STi_C200_ISS _00_02	24	0.98	11.7	0.478	911	205	2.43	353	TF
STi_C200_ISS _00_03	24	0.98	12.2	0.498	835	188	2.14	310	TF
STi_C200_ISS _00_04	24	0.98	12.1	0.494	905	203	2.34	339	TF
STi_C200_ISS _00_05	24	0.98	12.4	0.506	822	185	2.07	300	TF
Average					855	192	2.22	322	
S_{n-1}					49.3	11.1	0.155	22.5	
CV((%)					5.8	5.8	7.0	7.0	

2.4.4 Tensile Bond Strength

The purpose of this test is to determine the bond strength (i.e., pull off resistance) of the FRCM system, based on the application of the composite systems under control ambient conditions. Tests are performed as per AC434 Section 4.8 and reference standard ASTM C1583/C1583M-04. Five (5) bond specimens were tested per system under ambient laboratory conditions. The FRCM systems were applied on solid plain concrete blocks with nominal dimensions of 355 mm (14 in.) length, 100 mm (4 in.) width, and 100 mm (4 in.) thickness, with a single ply of each FRCM system fabric.

Regarding the substrate, the concrete 28-day compressive strength as determined by ASTM C39/C39M-14 (Standard Test Method for Compressive Strength of Cylindrical Concrete Specimens), was equivalent to 47.1 MPa (6840 psi), based on the average compressive strength of five concrete cylinders.

The FRCM systems were applied to the concrete surface as referenced in Section 2.2. After the curing process, a circular cut was made perpendicular to the surface using a diamond coring drill to a depth of 12.7 mm (0.5 in.) into the substrate. The test specimen was left intact, attached to the substrate. Any standing water was removed; the surface was cleaned from any debris from the drilling operation and was allowed to dry. A steel disk was then attached to the top FRCM surface using adhesive epoxy (Figure 2.4-12). The disk was centered with the test specimen and the axis of the disk was placed parallel to the axis of the test specimen. The epoxy adhesive was cured following the manufacturer's instructions prior to testing.

(a) (b) (c)

Figure 2.4-12 –Pull off test: a) drilling instrumentation; b) circular embedded cut; c) attached steel disk

The load was applied manually using the screw system of the test machine connected to a hydraulic piston. The test was performed under load control at a constant rate so that the tensile stress increased at a rate of 35 ± 15 kPa/s (5 ± 2 psi/s).

(a) (b)

Figure 2.4-13 –Pull off test instrumentation: a) James Bond tester; b) test set up

The ultimate bond or tensile strength was determined to be 1.92 MPa (280 psi) and 1.37 MPa (203 psi) for C600 and C200 FRCM systems, respectively.

Figure 2.4-14 shows the different possible failure modes during the bond test as per AC434. The primary failure mode of the bond tests occurred within the FRCM composite system, at the interface between the FRCM mortar and fabric, herein referred to as failure type "C" (Figure 2.4-15). The ultimate bond or tensile strength was calculated based on the type of failure, following the guidelines provided by AC434 by dividing the recorded tensile load at failure by area, where the area depends on the failure mode (net area or matrix area) of the test specimen.

Table 2.4-5 contains the tabulated bond (tensile strength) results with average, standard deviation (Std. Dev.) and coefficient of variance (C.O.V) values, where the following nomenclature was used:

A Area of test specimen (steel disk);
T_l Ultimate failure; and
T_S Ultimate bond or tensile strength

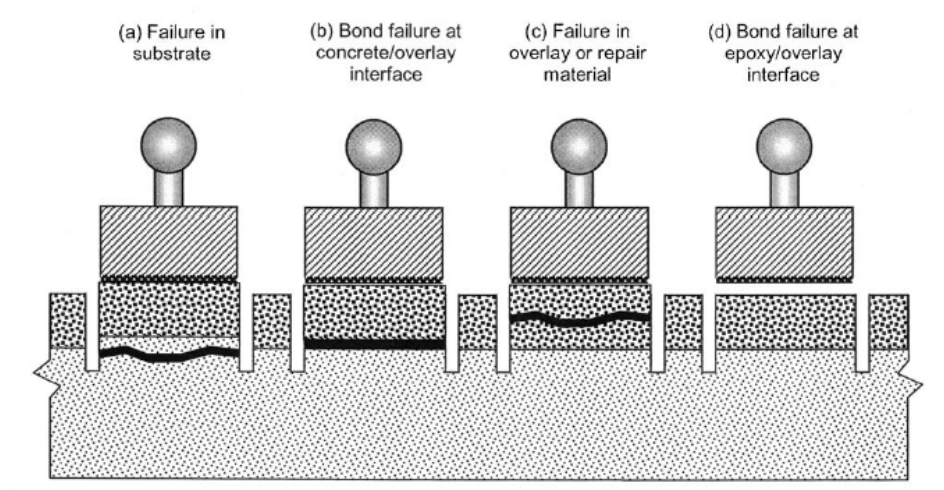

Figure 2.4-14 – Bond test failure mode types

Figure 2.4-15 – Representative failure mode of tension bond strength test

Table 2.4-5 – Tabulated results for tensile bond tests (ASTM D1583)

SPECIMEN ID	Time	Area		T_l		T_s*		Failure Mode
	sec	mm^2	in^2	N	lbf	MPa	psi	
STi_C600_BTC _001	32	1810	2.80	1780	400	0.98	143	B
STi_C600_BTC _002	62	1810	2.80	4495	1010	2.48	360	B
STi_C600_BTC _003	57	1810	2.80	3694	830	2.04	296	B
STi_C600_BTC _004	44	1810	2.80	3071	690	1.70	246	B/C
STi_C600_BTC _005	65	1810	2.80	4450	1000	2.46	357	D
Average				3498	786	1.93	280	
Sn-1				1007	226	0.56	81	
CV((%)				29	29	29	29	
STi_C200_BTC _001	42	1810	2.80	1891	425	1.05	152	B
STi_C200_BTC _002	54	1810	2.80	2670	600	1.48	214	B
STi_C200_BTC _003	43	1810	2.80	2670	600	1.48	214	B

SPECIMEN ID	Time	Area		T_l		T_S*		Failure Mode
	sec	mm^2	in^2	N	lbf	MPa	psi	
STi_C200_BTC _004	30	1810	2.80	1891	425	1.05	152	B
STi_C200_BTC _005	53	1810	2.80	3560	800	1.97	285	B
Average				2537	570	1.40	203	
S_{n-1}				619	139	0.34	50	
CV((%)				24	24	24	24	

3 RC BEAM EXPERIMENTS

Beams are divided into two phases: Phase I consisting of static tests where specimens are loaded monotonically to failure, and Phase II comprised of beams subjected to cyclic (fatigue) loading. The experimental parameters that will be investigated include: amount of supplemental reinforcement, ultimate strength, static failure mode, applied stress range, fatigue life, fatigue failure mode and residual strength. For members subject to cyclic loading, a stress ratio vs. number of cycles (S-N) curve is developed with the objective of defining the endurance limit for the strengthened beams.

3.1 Beam Design and Preparation

RC beams were designed per ACI 318-14 to be under-reinforced while exceeding the minimum flexural steel requirements and all beams contained shear reinforcement (stirrups) in order to prevent a shear failure. Figure 3.1-1 shows the beam geometry and reinforcement details where not all specimens contained externally bonded FRCM materials. RC beams were prepared by using wooden formwork to give the specimens the designated concrete shape and finish. The straight steel longitudinal bars and stirrups were tied together using steel ties and the final assembly took the form of a cage (Figure 3.1-2). After the formwork was prepared, RC beams and concrete cylinders were cast following ASTM C192/C192M-07 using Type I Portland cement. The beams and cylinders were left to cure for at least 28 days prior to testing and/or FRCM application. Figure 3.1-2 shows the steel cage and formwork prior to concrete casting. RC beams were designed with a nominal 28-day concrete compressive strength of 48.3 MPa (7 ksi) and design steel yield strength and elastic modulus of 413.7 MPa (60 ksi) and 200 GPa (29000 ksi), respectively, which are commonly-used nominal material properties. Twenty-seven RC beams were cast as shown in Figure 3.1-3.

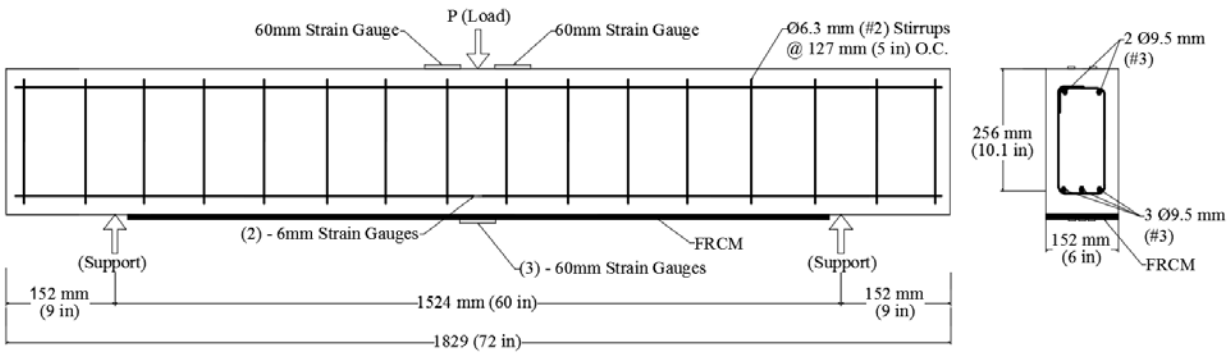

Figure 3.1-1– Reinforced concrete beam details

Figure 3.1-2–RC beam preparation

Figure 3.1-3–RC Beam concrete casting

3.2 Material Characterization

Experimental tests were performed to determine the material properties of concrete and steel reinforcement. Five concrete cylinders were tested in compression to with the maximum loads and

corresponding ultimate strengths are as summarized in Table 3.2-1. After 28 days, the average compressive strength of five concrete cylinders was 52.5 MPa (7.6 ksi) with a coefficient of variation (COV) of 2.65%. The typical failure mode for all concrete cylinders is shown in Figure 3.2-1.

The steel reinforcing bars were tested in tension as per ASTM A370. A clip-on extensometer with a 100 mm (4 in) gauge length was placed at mid-length of the specimen to measure strain. The yield strength was determined using the total extension under applied load. Table 3.2-2 contains a summary of tensile test results for five randomly selected steel samples. The average yield strength of the steel was 471 MPa (68 ksi) with a COV of 2.55%, and the average steel elastic modulus was 195 GPa (28,282 ksi) with a COV of 2.23%.

Table 3.2-1–Concrete compressive strength

Specimen ID	Max Load (kN)	Ultimate Strength (MPa)
C-COMP-1	421.7	52
C-COMP-2	443.7	54.7
C-COMP-3	413.3	51
C-COMP-4	432.3	53.3
C-COMP-5	415.8	51.3
Average	425.4	52.5
St. Dev.	11.3	1.4
COV	2.65%	2.65%

Figure 3.2-1–Concrete cylinders before and after compression test

Table 3.2-2 – Summary of steel tension tests

Specimen ID	Modulus of Elasticity		Yield Strength	
	GPa	ksi	MPa	ksi
S-Rebar-01	188.44	27330.90	459	66.57
S-Rebar-02	193.58	28076.98	493	71.50
S-Rebar-03	194.63	28229.99	475	68.89
S-Rebar-04	198.59	28803.04	463	67.15
S-Rebar-05	201.12	29171.00	467	67.73
Average	195.27	28321.51	471	68.31
St. Dev.	4.36	632.94	12	1.74
COV	2.23%		2.55%	

FRCM systems characteristics were also determined experimentally as presented in detail in Section 2. Table 3.2-3 summarizes the material properties including those of the FRCM systems used in RC beam experiment design (nominal), prediction and analysis. In an attempt to avoid confusion, Table 3.2-3 was developed to clearly present and distinguish between the two sets of material properties.

Table 3.2-3–Nominal and Experimental Material Properties

Material	Description	Nominal		Experimental	
		SI	US Customary	SI	US Customary
Concrete	28-Day Strength	f'_c= 48.3 MPa	f'_c= 7 ksi	f'_c = 52.5 MPa	f'_c = 7.61 ksi
Steel	Yield Strength	f_y = 413.7 MPa	f_y = 60 ksi	f_y = 471 MPa	f_y = 68.3 ksi
	Modulus of Elasticity	E_s=200 GPa	E_s=29000 ksi	E_s=195 GPa	E_s=28282 ksi
PBO FRCM	Ultimate Tensile Strength	f_{fe}= 1352 MPa	f_{fe}= 192.2 ksi	f_{fu}= 1664 MPa	f_{fu}= 241.3 ksi
	Cracked Elastic Modulus	E_f = 127.7 GPa	E_f = 18521 ksi	E_f = 127.7 GPa	E_f = 18521 ksi
	Ultimate strain	ε_{fe} = 0.012		ε_{fu} = 0.0176	
C600 FRCM	Ultimate Tensile Strength	f_{fe}= 1074 MPa	f_{fe}= 155.77 ksi	f_{fu}= 1394 MPa	f_{fu}= 202.2 ksi
	Cracked Elastic Modulus	E_f = 65.50 GPa	E_f = 9500 ksi	E_f = 65.50 GPa	E_f = 9500 ksi
	Ultimate strain	ε_{fe} = 0.012		ε_{fu} = 0.0164	
C200 FRCM	Ultimate Tensile Strength	f_{fe}= 799 MPa	f_{fe}= 115.9 ksi	f_{fu}= 1149 MPa	f_{fu}= 166.6 ksi
	Cracked Elastic Modulus	E_f = 65 GPa	E_f = 9427 ksi	E_f = 65 GPa	E_f = 9427 ksi

Ultimate Strain	$\varepsilon_{fe} = 0.012$	$\varepsilon_{fu} = 0.0123$

In Table 3.2-3, the effective FRCM tensile strain used for design, ε_{fe}, is defined as follows:

$$\varepsilon_{fe} = \begin{cases} \varepsilon_{fd} \leq 0.012 & \text{for FRCM failure} \\ \varepsilon_{cu}\left(\frac{d_f - c}{c}\right) - \varepsilon_{bi} \leq \min(\varepsilon_{fd}, 0.012) & \text{for concrete crushing} \end{cases}$$

Where ε_{fd} is the design FRCM strain defined as the average ultimate strain value minus one standard deviation as determined from the experimental material properties given in Table 2.4-2; and ε_{cu} is equal to a maximum compressive concrete strain of 0.003.

The design effective tensile strength is then determined to be $f_{fe} = E_f \varepsilon_{fe}$, where E_f is the same for the design and experimental modulus of elasticity taken from Table 2.4-2 with no reduction factor.

3.3 FRCM Configuration

To increase in flexural strength, the FRCM system is applied to the soffit of each beam. As the RC beam cracks, the neutral axis shifts upward and any concrete material below the neutral axis is assumed to provide no flexural resistance, while the steel carries the tension component of the internal moment couple. Placing FRCM on the soffit rather than the beam sides is ideal because the lever arm from the FRCM to the neutral axis is at its maximum.

FRCM application consists of rotating the beam 180 degrees in order to apply FRCM to the soffit. The design material properties were used in conjunction with ACI 549.4R-13 to determine theoretical design flexural capacities for various configurations of FRCM strengthening. The analysis was performed based on the given assumptions and possible failure modes specified in Section 11.1 of ACI 549.4R-13. It is noteworthy to mention that ACI549.4R limits the increase in flexural strength to 50% of the unstrengthened member ($\phi M_{n,\text{strengthened}} \leq 1.5\phi M_{n,\text{control}}$)

3.4 FRCM Application

The FRCM sequence of application is shown in Figure 3.4-1 . After sandblasting, the FRCM application was preceded by pressure washing the soffit of the concrete beams and removing any loose particles. The concrete substrate was maintained saturated-surface-dry prior to the application of the mortar. The mortar was prepared and applied using a trowel with a thickness of 3 to 4 mm (0.12 to 0.16 in) to the beam bottom face. 1.83 m (6 ft) long pre-cut fabrics were placed and embedded into the mortar with the primary direction (warp) orientated along the longitudinal

length of the beam. A trowel was used to embed the fabric into the matrix where a second layer of mortar of equal thickness was then applied to create a sandwich around the fabric. This procedure was repeated until the desired number of layers was applied. Beams with FRCM were left to cure for a minimum of 28 days prior to testing.

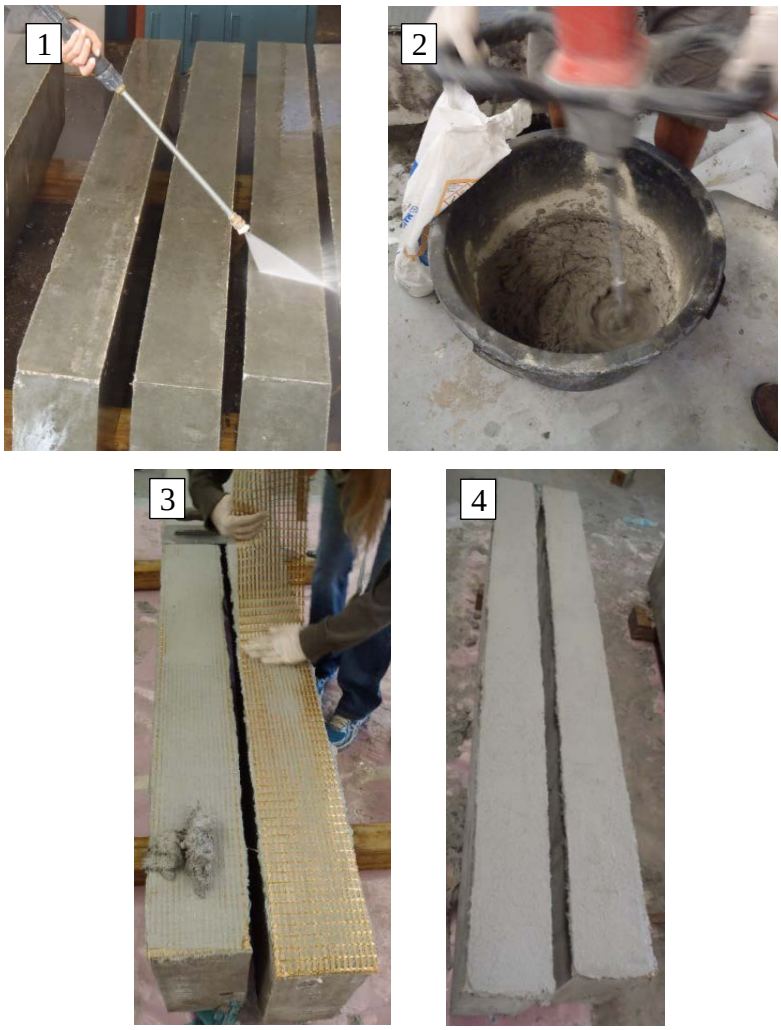

Figure 3.4-1– FRCM sequence of application: 1) water pressure cleaning; 2) mortar mixing; 3) fabric application 4) finished specimens

3.5 Tests Setup

A three-point bending test configuration with a 1.54 m (60 in) span was used for all specimens. Beams were instrumented with 6-mm (0.24 in) and 60-mm (2.36 in) strain gauges. Two 6-mm strain gauges applied to the center tension steel rebar measured tensile strain, two 60-mm gauges measured compressive strain in the concrete near midspan, and three 60-mm gauges measured tensile strain in the FRCM at midspan. In addition, three linear variable differential transducers

(LVDTs) were placed at midspan and each support to measure deflection and settlement. To prevent the unrealistic anchorage of the FRCM, a concrete grinder was used to cut the FRCM material adjacent to the supports so that the supports would not function as FRCM anchors. Figure 3.5-1 shows the test setup and instrumentation layout. Each specimen was tested with a 250-kN (55 kip) hydraulic actuator on a fatigue-rated test frame. The applied load was measured using an internal force transducer connected to the actuator.

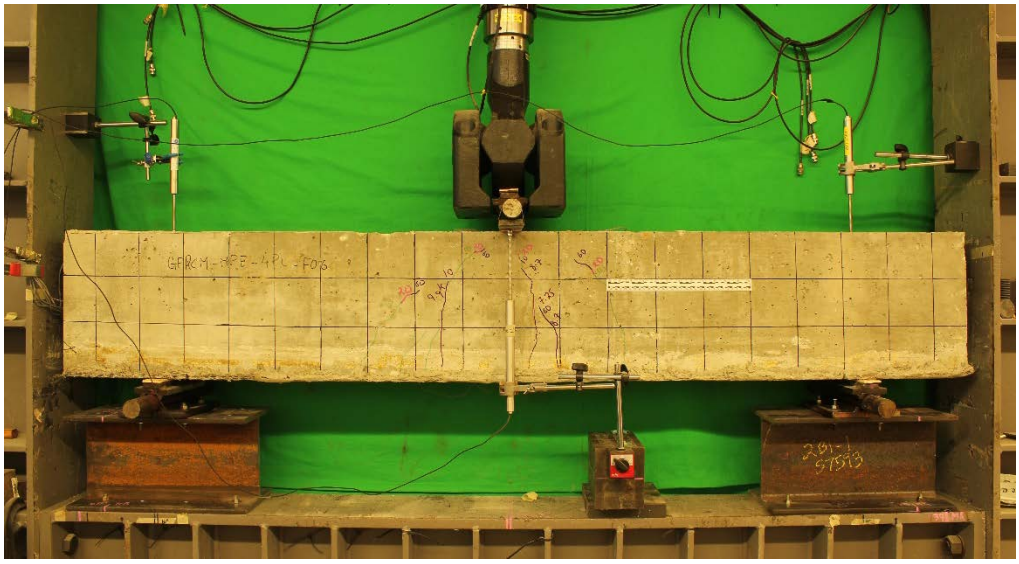

Figure 3.5-1–RC beam test setup

3.6 Experimental Procedure

Of the twenty-seven RC beams under evaluation, fifteen were used for PBO FRCM and twelve for Carbon FRCM experiments both sets divided into two phases. In Phase I, specimens were tested monotonically to failure. Phase II consisted of beams subjected to fatigue loading. All loading values were determined based on the steel yield and ultimate capacities.

3.6.1 Phase I

Beams in the first phase were tested at a load-controlled rate of 0.22 kN/sec (50 kip/sec) for PBO FRCM strengthened beams and displacement control rate of 0.0875 mm/sec (0.0034 in/sec) for Carbon FRCM strengthened beams with a total of 4 quasi-static loading and unloading cycles in each test. The maximum value for each loading cycle was determined to investigate beam performance before and after concrete cracking as well as before and after steel yielding. An

illustrative example of the load steps on PBO FRCM strengthened beams is presented in Figure 3.6-1. Beams in Phase I consist of nine beams in total. Five beams corresponded to the PBO FRCM system: two unstrengthened and three RC beams each strengthened with one, three, and five layers of fabric. Four beams corresponded to the Carbon FRCM system: one unstrengthened beam, one strengthened with two layers of C200 fabric and two strengthened with one and two layers of C600 fabric, respectively.

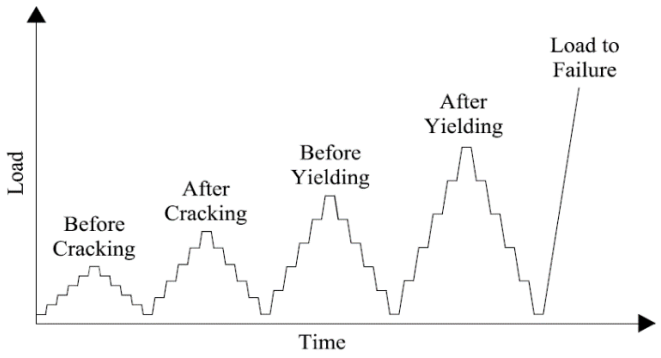

Figure 3.6-1– Typical loading cycles

3.6.2 Phase II

Phase II consisted of initially pre-cracking each beam and then applying a cyclic fatigue loading resembling that of a sine wave at a load rate of 2 Hz (2 cycles/sec). The reference value used herein is the theoretical static load at which yielding of the reinforcing steel occurs in the beam. All cyclic (fatigue) loads are comprised of maximum and minimum values, which are referred to a percentage of the static yield (PSY) load. Based on the simulation of a typical RC slab bridge designed according to AASHTO LFRD (2010), a minimum load value equivalent to 20 percent of the static yield (20 PSY) was used for all cyclic tests. Pre-cracking of each beam is done to simulate service condition and follows the same procedure as explained in Section 3.6.1-Phase I.

Previous studies have shown that RC beams subjected to fatigue loads experience failure mainly due to fatigue rupture of the steel reinforcement and less commonly by fatigue failure of the concrete (Chang and Kesler 1958, Corley et al. 1978, Helagson and Hanson, 1978). Therefore, it is necessary to address the fatigue limitations for steel provided by ACI 215R-97 and AASHTO LRFD (2010). For a minimum load of 20 PSY, a corresponding stress in the steel of 94 MPa (13.6 ksi) is induced. ACI 215R-97 and AASHTO LRFD (2010) specify an allowable stress range of 138 MPa (20 ksi) and 162 MPa (23.5 ksi), respectively. These values correspond to peaks of load

of 50 and 55 PSY. Thus, if the applied maximum stress is less than 50 PSY, there should be no failure in the steel reinforcement up to 2 million cycles. However, if the maximum applied stress is larger than 55 PSY, there is a likelihood that the steel may fail due to fatigue before reaching 2 million cycles.

In addition for FRCM strengthened RC members, ACI 549.4R-13 limits the tensile stress in the steel reinforcement to be 80 PSY during service loading, but this number has yet to be experimentally verified.

Thus, maximum stress values in the steel reinforcement were chosen for this research program to be larger than the maximum permitted values specified by ACI 215R-97 (50 PSY) and AASHTO LRFD 2010 (55 PSY) and such to establish if the ACI 549.4R-13 (80 PSY) threshold could be experimentally verified.

It is also necessary to ensure that concrete stresses do not exceed the fatigue provisions specified by ACI 215R-97. For the given beam cross-section configuration, a steel stress of 20 PSY corresponds to a concrete stress of 4.9 MPa (0.7 ksi), which is less than 10% of the concrete compressive strength ($f`_c$) while the allowable stress is 45% of $f'_c$. Thus, all maximum load values were chosen to induce concrete stresses less than the threshold of 45% of the concrete compressive strength ($f`_c$). Accordingly, the highest peak load generating 90 PSY corresponds to a theoretical maximum concrete compressive stress of 40% $f`_c$ and maximum FRCM tensile stress of 335 MPa (48.5 ksi), which is 23% of f_{fd}, as shown in Figure 3.6-2. Note that the tensile stress in the FRCM satisfies the fatigue limit of 30% f_{fd} prescribed by ACI 549.4R-13.

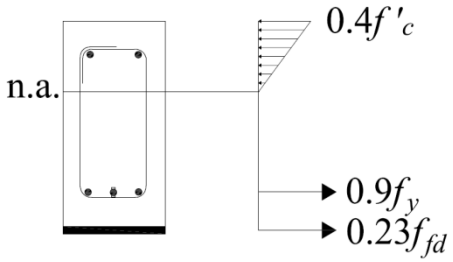

Figure 3.6-2– Stress distribution for FRCM strengthened beam subject to a load generating 90 PSY

Table 3.6-1 summarizes the test matrix for PBO FRCM strengthened beams while Table 3.6-2 is relative to Carbon FRCM strengthened beams. All cyclic loads were applied until failure of the specimen or 2 million cycles, whichever occurred first. All beams that reached a fatigue life of 2

million cycles were re-tested quasi-statically to determine the post-fatigue residual strength. The same load procedure used for Phase I static tests was used for the Phase II residual static tests. Table 3.6-1 and Table 3.6-2 contain a description of each specimen of Phases I and II, which are labeled using the "*A–B–C-D*" format, where "*A*" represents the test type (F for Fatigue and S for Static), "*B*" represents the beam type (CON for control beams, and PBO, C200 and C600 for PBO or Carbon strengthened beams), "*C*" denotes the number of fabric layers applied (1P for one layer, 3P for three layers, and 5P for five layers), and "*D*" represents the maximum cyclic load value (e.g., 75 for 75PSY) for fatigue tests.

Table 3.6-1—Test matrix for PBO FRCM strengthened beams of Phase I and II

Specimen ID	Load Type	External Reinforcement	Max Load (PSY)
S-CONa	Static	None	-
S-CONb			
S-PBO-1P		1 Layer	
S-PBO-3P		3 Layers	
S-PBO-5P		5 Layers	
F-PBO-3P-90	Cyclic (Fatigue)	3 Layers	90
F-PBO-3P-85			85
F-PBO-3P-80a			80
F-PBO-3P-80b			
F-PBO-3P-75a			75
F-PBO-3P-75b			
F-CON-0-75a		None	75
F-CON-0-75b			
F-PBO-1P-75		1 Layer	75
F-PBO-5P-75		5 Layers	75

Table 3.6-2– Test matrix for Carbon FRCM strengthened beams of Phase I and II

Specimen ID	Load Type	External Reinforcement	Max Load (PSY)
S-CON	Static	None	-
S-C600-1P		1 Layer	
S-C600-2P		2 Layers	
S-C200-2P		2 Layers	
F-C200-2P-75	Cyclic (Fatigue)	2 Layers	75
F-C200-2P-70			70
F-C200-2P-65			65
F-C200-2P-60			60
F-CON-0-75		None	75
F-C600-2P-75		2 Layes	75
F-C600-2P-70			70
F-C600-2P-65			65

3.7 Experimental Results

3.7.1 Phase I Results

Results of Phase I experiments for each material system are presented and discussed in this section. Both PBO and Carbon FRCM systems share the same mode of failure under monotonic loading, that is dependent on the number of fabric layers. For FRCM strengthened specimens, crack bridging and consequently delayed crack openings with respect to the unstrengthened beams was observed.

A comparison of PBO FRCM strengthened load-deflection curves for the Phase I tests is given in Figure 3.7-1. Similarly, a summary of all experimental ultimate load values are given in Table 3.7-1, where S-CON* denotes the average of specimen S-CONa and S-CONb. The theoretical values are determined using the experimental material properties. The strength enhancement is the ratio of FRCM strengthened member to the average benchmark value and all experimental results were compared to theoretical values.

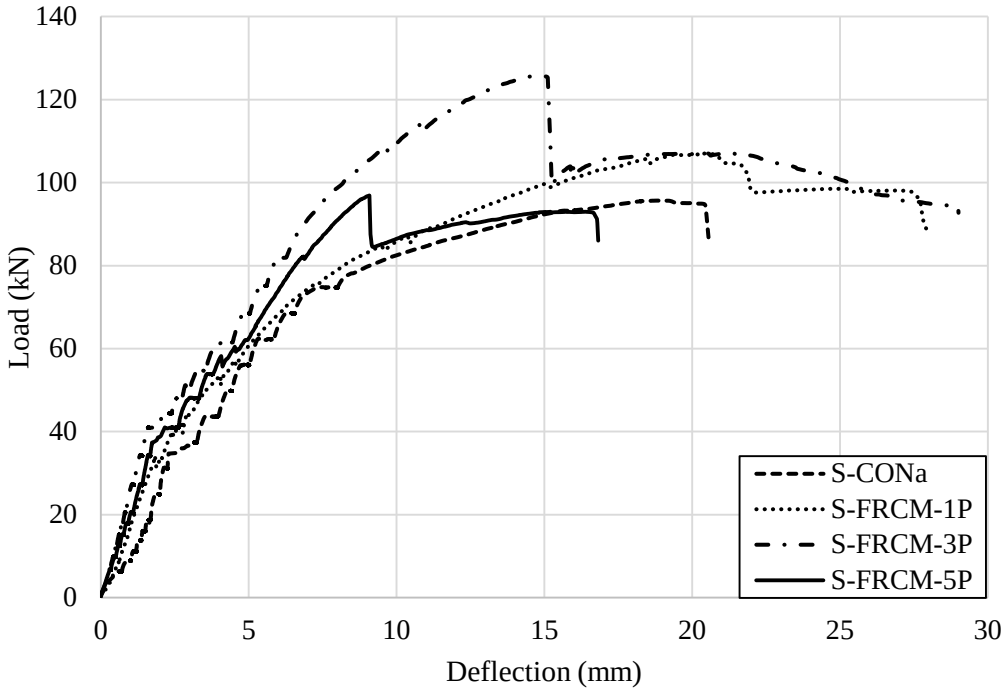

Figure 3.7-1– Load vs. deflection for Phase I PBO FRCM beams

All five beams exhibited similar behavior up to concrete cracking where the cracking load was not significantly affected by the FRCM presence. All FRCM strengthened specimens displayed a

greater post cracking stiffness than the benchmark specimens up to steel yielding, with S-FRCM-3P showing the greatest stiffness increase followed by S-FRCM-5P and S-FRCM-1P. All FRCM strengthened specimens exhibited an increase in static yield relative to the benchmark specimens. The greatest static yield value was observed in S-FRCM-3P followed by S-FRCM-5P, and S-FRCM-1P. Figure 3.7-2 shows the typical failure modes of the strengthened and unstrengthened beams that was mentioned earlier in this section.

Table 3.7-1– Static tests results for PBO FRCM strengthened beams: ultimate load (P_u)

Specimen ID	Theoretical		Experimental			Experimental/ Theoretical
	$P_{y,Th}$		$P_{u,avg}$		Enhancement $P_{u,strengthened}/P_{u,control}$	$P_{u,avg}/P_{u,Th}$
	kN	*kip*	*kN*	*kip*		
S-CON*	89.5	20.12	97.1	21.8	1	1.08
S-PBO-1P	90	20.23	107.02	24.06	1.1	1.19
S-PBO-3P	112	25.18	125.7	28.26	1.29	1.12
S-PBO-5P	134	30.124	96.9	21.78	1	0.72

a)

b)

Figure 3.7-2– Typical failure modes forPhase I static test specimens: a) S-CONa b) S-PBO

Figure 3.7-3 graphically sums the Phase I monotonic tests on Carbon FRCM strengthened beams where unlike the previous series of tests, these tests were all conducted in displacement-control mode, with four cycles of loading and unloading before increasing the displacement up to the failure as discussed earlier in Section 3.6.1. All the values in the graph reflect experimental data and therefore no design or reduction factor is applied. Static test results are summarized in Table 3.7-2 that compares the theoretical and experimental ultimate capacities and Figure 3.7-4 shows the typical failure mode of the Carbon FRCM strengthened beams that is similar to that of PBO FRCM strengthened beams discussed earlier.

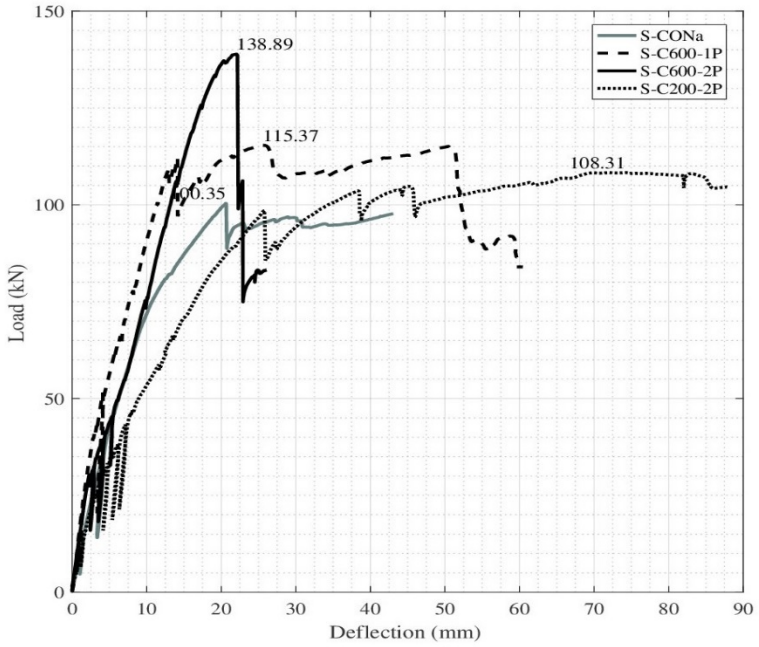

Figure 3.7-3–Load vs. deflection for Phase I Carbon FRCM specimens

Table 3.7-2– Static Tests Results for Carbon FRCM strengthened beams: ultimate load (P_u)

Specimen ID	Theoretical		Experimental			Experimental/ Theoretical
	$P_{y,Th}$		$P_{u,avg}$		Enhancement $P_{u,strengthened}/P_{u,control}$	$P_{u,avg}/P_{u,Th}$
	kN	*kip*	*kN*	*kip*		
S-CON	62	13.94	100.35	22.56	1	1.19
S-C600-1P	70	15.74	115.36	25.93	1.15	1.22
S-C600-2P	74	16.64	138.89	31.22	1.38	1.24
S-C200-2P	69	15.51	108.31	24.35	1.08	1.37

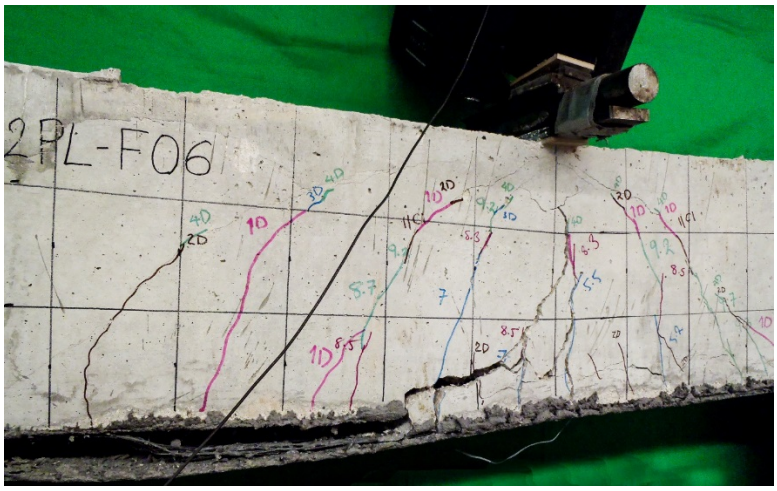

Figure 3.7-4 – Typical Failure Modes for Phase I static test Carbon FRCM specimens

3.7.2 Phase II Results

All beams in Phase II were subjected to cyclic loading. RC beams strengthened with one, three and five layers of PBO FRCM or two layers of either C200 or C600 Carbon FRCM were tested with descending maximum load values, in an attempt to determine an endurance limit based on the level of stress in the reinforcing steel. Once the endurance limit was determined, unstrengthened RC beams were tested at this limit for comparison. The failure type, number of cycles to failure (fatigue life), and residual maximum load values are summarized in Table 3.7-3 for PBO FRCM strengthened beams and in Table 3.7-4 for Carbon FRCM strengthened beams.

Table 3.7-3– Summary of PBO FRCM Phase II fatigue results

Specimen ID	Max % static yield (PSY)	Failure Type	Number of Cycles at failure $\times 10^6$	Residual Max Load $P_{u.R}$ Kn (kip)	Residual/ Experimental $P_{u.R}/P_{u.avg}$
F-CON-0-75a	75	Steel Fracture	0.919	-	-
F-CON-0-75b		Steel Fracture	1.46	-	-
F-PBO-3P-90	90	Steel Fracture	0.492	-	-
F-PBO-3P-85	85	Steel Fracture	0.562	-	-
F-PBO-3P-80a	80	None	2	131.7 (29.6)*	1.05
F-PBO-3P-80b		Steel Fracture	1.89	-	-
F-PBO-3P-75a	75	None	2	124.5 (27.99)*	0.99
F-PBO-3P-75b		None	2	119.8 (26.93)*	0.95
F-PBO-1P-75		Fabric Slippage w/in Matrix	0.962	-	-
F-PBO-5P-75		None	2	102.4 (23.02)*	1.06

**Maximum load from monotonic load test performed after 2M cycles of fatigue loading*

Table 3.7-4– Summary of Carbon FRCM Phase II fatigue results

Specimen ID	Max % static yield (PSY)	Failure Type	Number of Cycles at failure $\times 10^6$	Residual Max Load $P_{u.R}$ kN (kip)	Residual/ Experimental $P_{u.R}/P_{u.avg}$
F-CON-0-75	75	Steel Fracture	0.824	-	-
F-C200-2P-75	75	Steel Fracture	1.334	-	-
F-C200-2P-70	70	Steel Fracture	1.231	-	-
F-C200-2P-65	65	None	2	107.6 (24.19)*	0.99
F-C200-2P-60	60	None	2	102.4 (23.02)*	0.95
F-C600-2P-75	75	Steel Fracture	1.526	-	-
F-C600-2P-70	70	Steel Fracture	1.959	-	-
F-C600-2P-65	65	None	2	131.6 (29.58)*	0.95

**Maximum load from monotonic load test performed after 2M cycles of fatigue loading*

3.7.3 Residual Stress

The residual to experimental ratio is defined as the ratio of residual maximum load ($P_{u.R}$) to the average maximum load ($P_{u.avg}$) for the statically tested virgin beams given in Table 3.7-1 and Table 3.7-2. All results and observations including: fatigue life, fatigue behavior, failure modes, and residual strength are discussed where an S-N curve is then presented. The strain gauges applied to the steel reinforcing bars failed during the tests producing unusable data.

As expected, the fatigue life of the strengthened beams decreases by increasing the maximum applied stress to the steel rebars. The shortest fatigue life was observed in PBO FRCM strengthened specimen with 20~90 PSY applied stress that exceeded the AASHTO LRFD (2010) safe range of applied stress on steel rebars. From the experience gained through experiments on PBO FRCM strengthened specimens, authors limited the applied stress on Carbon FRCM ones to maximum 75 PSY for the sake of efficiency and economy. An important outcome to be highlighted is the result of residual strength on those specimens that went through 2 million cycles without failure. No significant reduction of capacity due to fatigue cycling compared to the static benchmark tests was observed. Residual strength of the specimens who survived two million cycles of fatigue loading along with the monotonic test results of Phase I specimens of strengthened and unstrengthened beams are shown in Figure 3.7-5 for 3-layer PBO FRCM strengthened specimens and in Figure 3.7-6 for 5-layer ones.

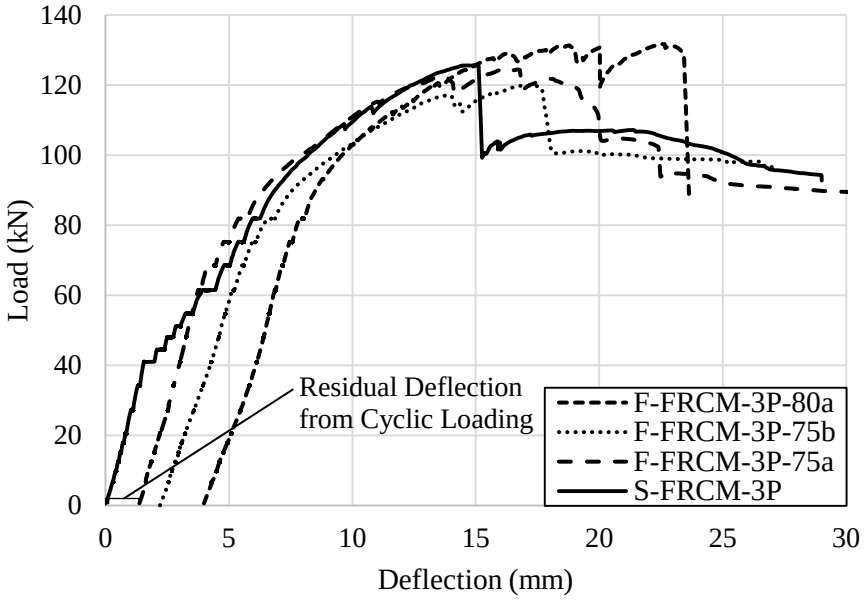

Figure 3.7-5– Load vs. deflection curves for residual static tests on 3-layer PBO FRCM beams

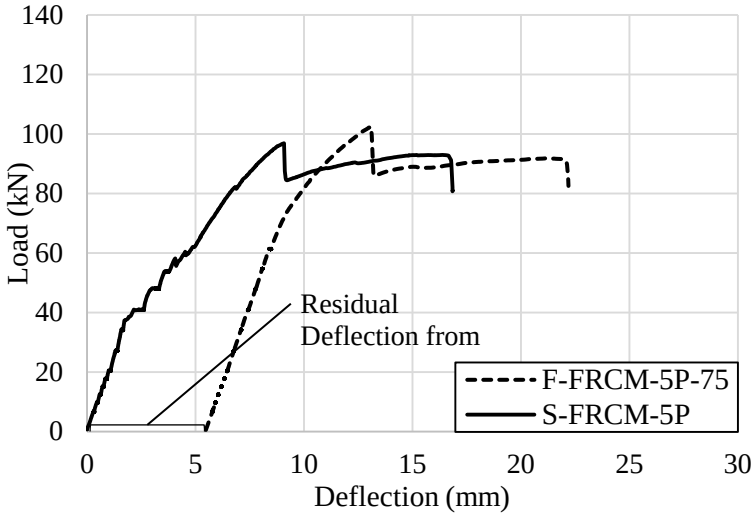

Figure 3.7-6– Load vs. deflection curves for residual static tests on 5-layer PBO FRCM beams

The residual strength graphs are shown in Figure 3.7-7 for Carbon FRCM strengthened beams.

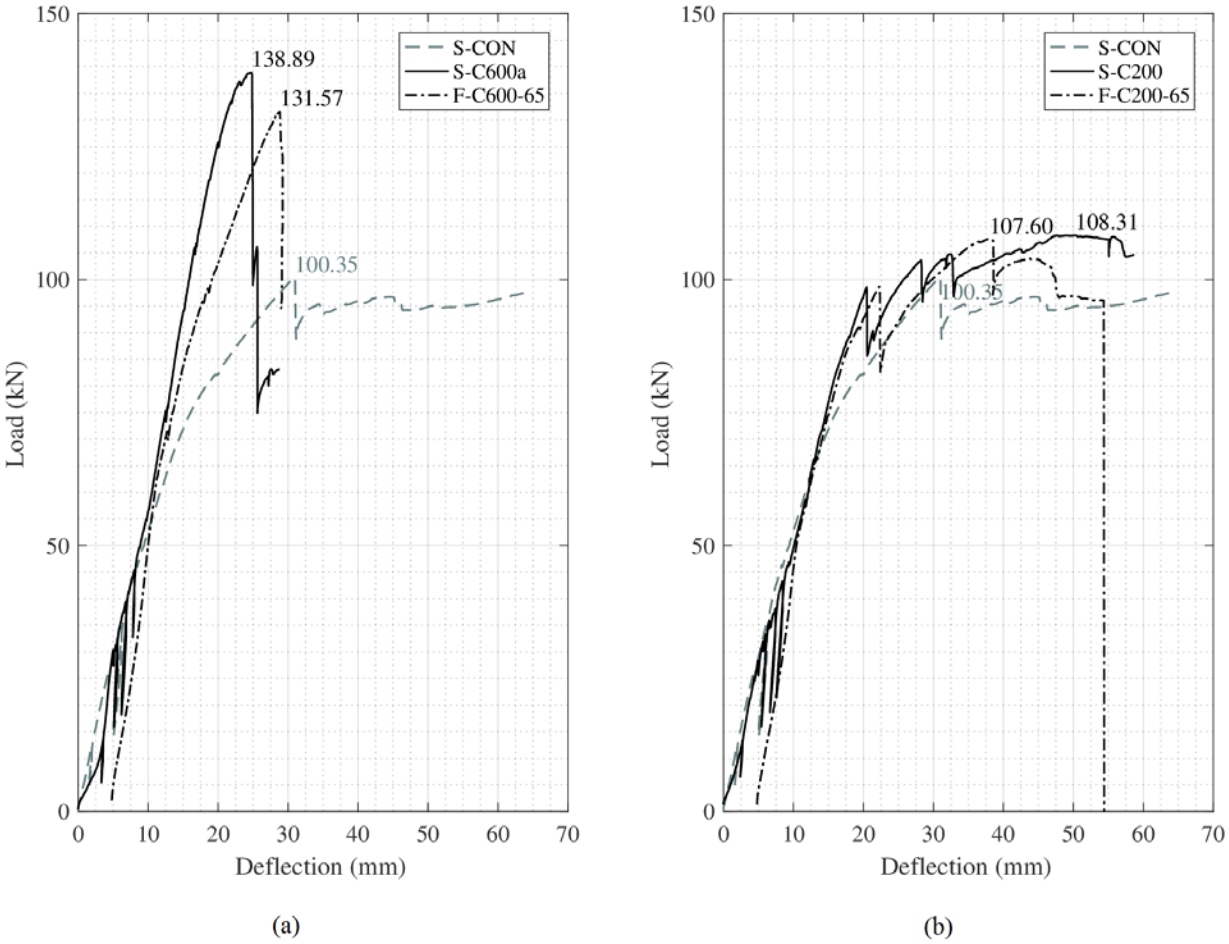

Figure 3.7-7– Load vs. deflection curves for residual static tests on Carbon FRCM beams: a) C600 FRCM; b) C200 FRCM

3.7.4 Failure Mode

For FRCM specimens subjected to cyclic loading, the primary failure mode was due to fatigue rupture of steel reinforcement followed by delamination of the FRCM layers starting from intermediate cracks and propagating outwards, and concrete crushing as shown in Figure 3.7-8.

Figure 3.7-8– Typical fatigue failure mode for Phase II beams

3.7.5 S-N Curves

Finally, the Stress Ratio versus the Number of Cycles known as S-N curves for both FRCM material systems are plotted in Figure 3.7-9 and Figure 3.7-10 where the arrows show those specimens that endured two million cycles and were tested for the residual stress. Specimens without arrow failed under fatigue loading.

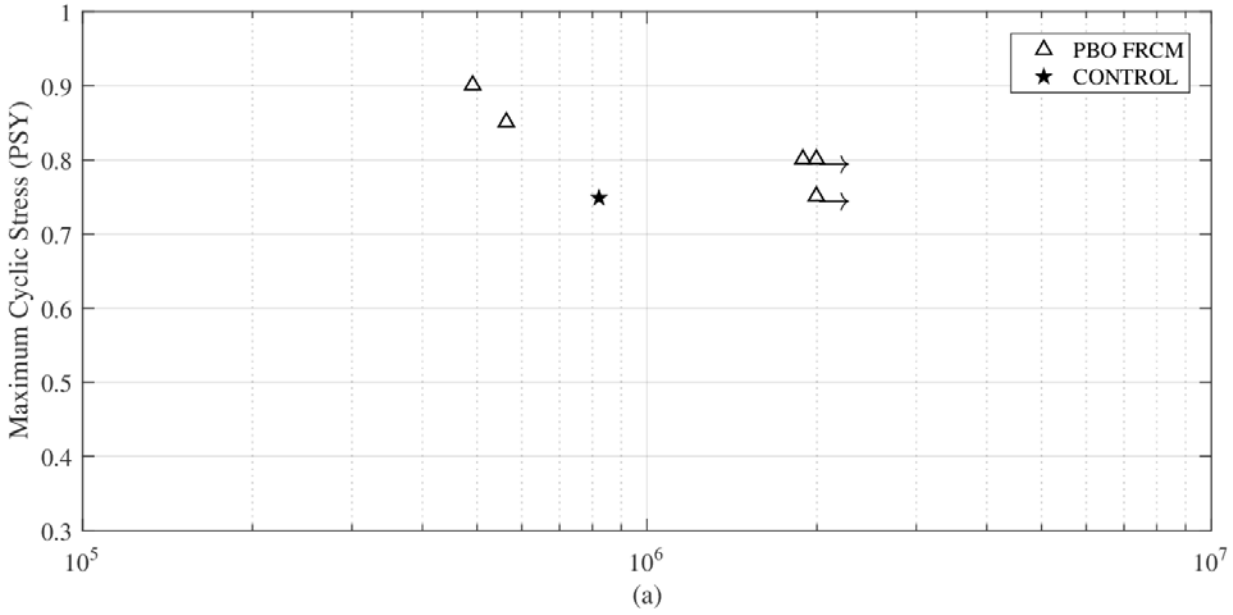

Figure 3.7-9– S-N Diagram for 3-Layers PBO FRCM

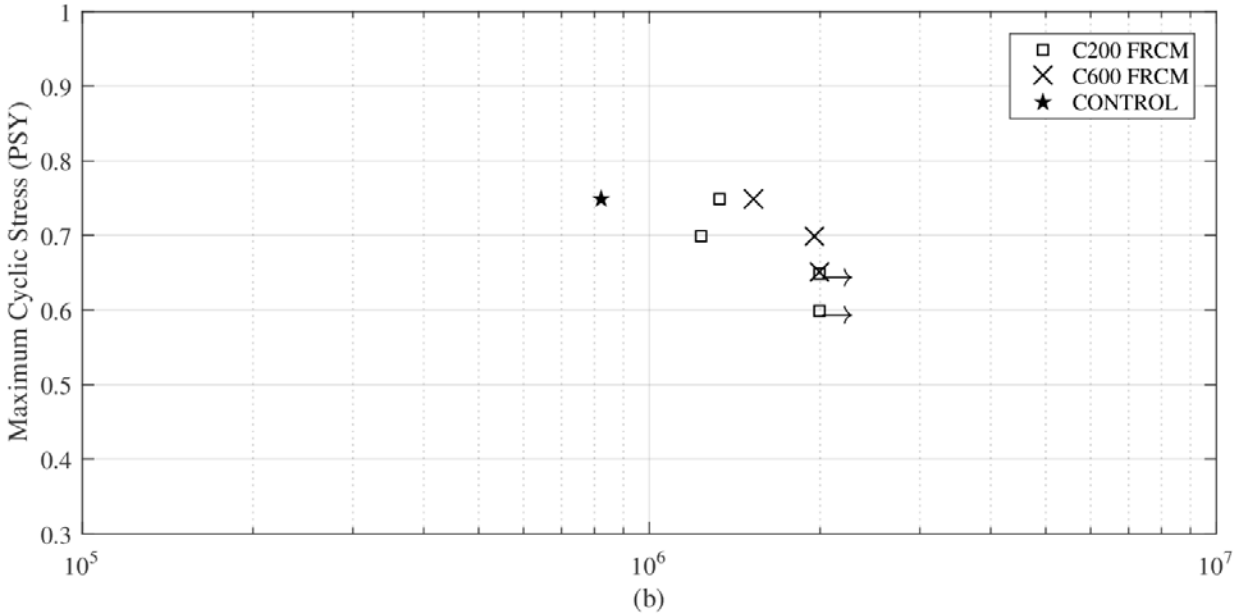

Figure 3.7-10– S-N Diagram for 2-Layers Carbon FRCM

4 DISCUSSION AND CONCLUSIONS

4.1 Materrial Characterization

Material characterization test results of Carbon FRCM systems were presented in Chapter 2 while the ones relative to PBO FRCM were simply referenced. The tensile tests for system caharacterization conducted herein follow the protocol of Acceptance Criteria AC434-2013 that allows for fibers to slip inside the matrix mortar within the grips. Because of applied boundary conditions in the test configuration, failure mechanism starts with debonding of fibers from their surrounding matrix mortar at the micro level due to bond shear stresses that lead to slippage of fibers within the matrix. This slippage allows the matrix mortar to axially deform under tensile stresses up to a point that the surface energy required to initiate a crack is attained and cracks develop in the matrix. Consequently, the released energy of the cracked surface transfers to the bridging fibers through frictional (and to a smaller degree to chemical bond) stresses and since the fibers have notably higher strength and strain capacity than the mortar matrix, the overall fracture toughness of the system in the vicinity of crack increases. This is a phenomenon known as fracture toughening (Marshall et al., 1985).

During the tests, it was observed that multiple cracks generate and propagate within monitored length of the coupon. Multiple cracks which accommodate higher overall displacement and strain up to failure (that govern the system stiffnes or elastic modulus) are formed due to the fact that the combination of chemical and frictional bond capacity at the fiber-matrix interface near the first crack exceeds the critical stress required to generate a fracture in the matrix.

4.2 Satic and Cyclic Beam Tests

The overall failure of the beams tested quasi-statically was mainly due to interlaminar delamination of the fibers for PBO FRCM and debonding for Carbon FRCM systems for the fiber area ratio and fabric architecture of the selected systems. The results obtained need to be valdated of other FRCM system.

This failure mode matches the results of the tensile bond tests covered in Section 2.4.4 showing that the dominant bond failure mode was reported type (b), at the FRCM-substrate interface. Authors aknowledge that there may exist other FRCM faiure modes (that did not occur in this

study) such as the one due to fiber rupture, in case of fabrics with lower reinforcement ratios and moduli.

The effectiveness of the selected FRCM systems was studied when applied to RC beams during Phase I tests in Chapter 3. It was assumed that the most influential parameters that could potentially affect the flexural behavior of the FRCM systems were reinforcement ratio and the fabric architecture. Therefore, PBO FRCM reinforcement ratio was a variable to be investigated in the study using one, three and five layers of fabric. Moreover, two different fabric architectures were used for the Carbon FRCM systems that provide different reinforcement ratios, but the number of layers were kept constantly equal to two. The benefits of FRCM materials as a strengthening solution for flexural members is well-known (Babaeidarabad et al., 2014; Pino and Nanni 2015) and was observed in the test results herein for both material systems.

Experimental results indicate that the flexural performance of the FRCM strengthened RC members is highly dependent on the reinforcement ratio and startlingly, increasing the fiber ratio by adding number of layers not always is beneficial and there exists a threshold after which the increase in the reinforcement ratio will result in a relative reduction of flexural capacity of the member. For instance, PBO FRCM strenghtened beams under monotonic loading discussed in Section 3.6.1 show a poor performance when strengthened with five layers with respect to those strengthened with three layers by a large margin. This apparent abnormality can be explained considering that the ultimate bond strength of matrix mortar is a constant value regardless of the reinforcement ratio. By adding layers of fabric, the total stiffness of the FRCM system will increase and so does its proportional distributed stress. However, the induced flexural moment on the beam has to transfer to the FRCM system through shear bond stresses at the concrete-FRCM and fiber-matrix interfaces and so the beam will withstand a relatively lower bending moment.

Fatigue failure of the RC beams was associated predominantly with fatigue behavior of steel reinforcement while no fatigue failure in the concrete and FRCM fabric was observed. S-N curves suggest that the FRCM can improve the fatigue life of the strengthened memebrs most probably because the characteristic values of FRCM system obtained through AC434-2013 tests are slightly underestimated and the material performs better in structural members. The actual stress in reinforcing steel of strengthened beams is slightly lower than what is analytically calculated and strengthened beams comparatively endure higher number of cycles.

Residual strength of the beams which withstood two million cycles of load indicate almost no reduction in flexural capacity compared to the benchmark virgin RC beams which confirms the validity of the endurance limits found for each system in this project.

5 REFERENCE

Babaeidarabad, S., Arboleda, D., Loreto, G. & Nanni, A. (2014). "Flexural Strengthening of RC Beams with an Externally Bonded Fabric-Reinforced Cementitious Matrix", Journal of Composites for Construction, 18(5), 4014009.

Chang, T. S., & Kesler, C. E. (1958). “Fatigue behavior of reinforced concrete beams”. In Journal Proceedings (Vol. 55, No. 8, pp. 245-254).

Corley, W. G., Hanson, J. M., & Helgason, T. (1978). Design of reinforced concrete for fatigue (No. RD059. 01D).

Helagson, T., & Hanson, J. M. (1974). Investigation of design factors affecting fatigue strength of reinforcing bars-statistical analysis. Special Publication, 41, 107-138.

Marshall, D. B., Cox, B. N., & Evans, A. G. (1985). The mechanics of matrix cracking in brittle-matrix fiber composites. Acta Metallurgica, 33(11), 2013-2021.

Pino, V., and Nanni, A. (2015). “Repair of Damaged PC Girder with FRCM and FRP Composites,” Publication No. 00042134-04, Grant No. DTRT13-G-UTC45, USDOT RE-CAST University Transportation Center, 88. Missouri S&T, Rolla, MO.